Journal of Peridynamics and Nonlocal Modeling (2022) 4:303–335
https://doi.org/10.1007/s42102-022-00080-7

ORIGINAL ARTICLES

Analytical Solutions of Peridynamic Equations. Part I: Transient Heat Diffusion

Ziguang Chen[1,2] · Xuhao Peng[1] · Siavash Jafarzadeh[3] · Florin Bobaru[3]

Received: 3 August 2021 / Accepted: 24 February 2022 / Published online: 21 March 2022
© The Author(s), under exclusive licence to Springer Nature Switzerland AG 2022

Abstract
In this paper, we construct formal analytical solutions for peridynamic models of transient diffusion using the separation of variables technique. We show that the infinite series nonlocal solutions can be obtained directly from corresponding classical solutions by inserting "peridynamic (nonlocal) factors" in the time-exponential part of the solution. We find analytical expressions for the nonlocal factor. In 2D rectangular domains, these can be written in terms of Bessel functions. The nonlocal factor depends on the horizon size and converges to value one as the horizon size goes to zero, recovering the classical form of the solution for the corresponding partial-differential equations. We also show that, as time goes to infinity, the nonlocal solution converges to the classical one, for a fixed horizon. We consider examples of transient diffusion problems with Dirichlet and Neumann boundary conditions. Their analytical solutions are compared with the corresponding classical solutions. While most of the analytical solutions we present here are formal, for a number of cases, we are able to prove uniform convergence of the series solutions. This is the first contribution that presents analytical (formal) solutions to peridynamic transient diffusion problems in 1D or 2D finite domains by separation of variables, with arbitrary boundary conditions, and shows their connections to the corresponding solutions to the classical/local problem.

Keywords Peridynamics · Separation of variables · Analytical solutions · Nonlocal factor · Diffusion · Transient heat transfer

✉ Ziguang Chen
zchen@hust.edu.cn

✉ Siavash Jafarzadeh
sia.jafarzadeh@gmail.com

✉ Florin Bobaru
fbobaru2@unl.edu

[1] Department of Engineering Mechanics, School of Aerospace Engineering, Huazhong University of Science and Technology, Wuhan 430074, China

[2] Hubei Key Laboratory of Engineering Structural Analysis and Safety Assessment, 1037 Luoyu Road, Wuhan 430074, China

[3] Department of Mechanical and Materials Engineering, University of Nebraska-Lincoln, Lincoln, NE 68588-0526, USA

1 Introduction

Two decades ago, Silling introduced the peridynamic (PD) theory, a spatial integral-type alternative of the classical continuum mechanics [1]. Allowing displacement discontinuities in the theory, the PD model can treat fracture and damage as natural parts of its solution process. A fundamental generalization of the original peridynamic theory beyond pair-wise interaction between material points was published in 2007 [2]. Peridynamics is particularly well suited for dealing with cracks and damage, especially in situations where the crack paths are not known in advance. PD models have been successfully applied to simulate dynamic fracture [3, 4], corrosion damage and stress corrosion cracking [5–7], thermally driven cracks [8], multiphase transport [9], etc.

The PD formulation is based on nonlocal interactions between material points in a continuum. The interaction between a material point and its neighbors extends beyond the nearest neighbors, over a region called "the horizon." The relation between peridynamics and the conventional differential formulation and convergence of the numerical computation of peridynamics itself have been analyzed mathematically [10–12]. Convergence in PD can be defined in several ways: convergence in terms of the horizon size (δ) going to zero, with the limit being the classical, PDE-based formulation of the problem [12, 13], and numerical convergence for a fixed horizon size, in terms of increasing the number of nodes inside the horizon region [14]. The numerical PD approximation will converge to the exact nonlocal PD solution for the given δ, when the number of nodes inside the horizon region goes to infinity.

It has long been thought that obtaining analytical solutions for peridynamic models is more difficult than for corresponding PDE-based models, since the PD formulations lead to integro-differential equations for which analytical solutions are not readily available. For special types of peridynamic problems, analytical solutions have been reported in the literature. However, we found these solutions to be limited to problems set in infinite domains: static and dynamic elastic response [15–18], propagation of solitary waves [19] and of defects [20] in 1D infinite bars. We have not found analytical solutions to PD problems posed in a finite domain in the literature.

In this paper, we show how to obtain formal analytical solutions of PD equations for transient diffusion problems in finite 1D and 2D domains using the method of separation of variables. In a few cases, we prove uniform convergence of solutions. The methodology follows closely that used in obtaining series solutions for the classical, PDE-based models of transient diffusion. The solutions to the PD equations satisfy the initial conditions and the local boundary conditions (and a particular extension to nonlocal boundary conditions) posed for the corresponding classical formulations of diffusion problems.

The paper is organized as follows: in Sects. 2 and 4, we show how the separation of variables method can be used to generate analytical solutions to linear peridynamic transient diffusion problems in finite one- and two-dimensional domains; Sects. 3 and 5 discuss convergence properties of solutions obtained for 1D and 2D problems, respectively, with Dirichlet and Neumann boundary conditions; we pay special attention to the nonlocal factor and its role on convergence properties, and a detailed proof of uniform convergence for a particular case is included in Appendix 2; in Sect. 6, we answer the question: given a nonlocal factor, what is the kernel generated by it and what is the corresponding solution to the transient diffusion problem defined by such a kernel? Sect. 7 contains concluding remarks.

In part II of this work [21], we show how to obtain analytical solutions to peridynamic models for elastodynamic problems.

2 Analytical Solutions for 1D Linear Peridynamic Transient Diffusion in a Finite Domain

2.1 Separation of Variables for 1D Peridynamic Diffusion

The 1D linear PD transient diffusion equation can be expressed as:

$$\frac{\partial u(x,t)}{\partial t} = D\mathcal{L}_\delta u(x,t) \tag{1}$$

where $u(x,t)$ is the unknown function (e.g., temperature for heat transfer problems, concentration for mass diffusion) of position x, and time t. D is the material diffusivity, and $\mathcal{L}_\delta$ denotes the PD Laplacian operator, defined by:

$$\mathcal{L}_\delta u(x,t) = \int_{\mathrm{H}_x} \mu\big(|\widehat{x}-x|\big)\big[u\big(\widehat{x},t\big) - u(x,t)\big]\mathrm{d}\widehat{x} \tag{2}$$

an integral over a finite size neighborhood of x: H_x (the "horizon region"), which, in 1D, is a line segment centered at x of length 2δ. We refer to δ as the *horizon size* or simply the horizon. μ is the *kernel* function with $\mu = \mu(|\xi|)$, that has the support H_x; therefore, $\mu(|\xi|) = 0$ for $|\xi| > \delta$, where $\xi = \widehat{x} - x$.

Inspired by the derivation of formal analytical solutions for problems described by partial differential equations (PDEs) [22], we use the method of *separation of variables* to find analytical solutions for Eq. (1), subjected to initial and (local) boundary conditions. We seek, therefore, a solution to Eq. (1) in the form of a product:

$$u(x,t) = \mathrm{X}(x)\mathrm{T}(t) \tag{3}$$

Substituting Eq. (3) into Eq. (1) gives:

$$\mathrm{X}(x)\mathrm{T}'(t) = D\mathrm{T}(t)\mathcal{L}_\delta \mathrm{X}(x) \tag{4}$$

where the prime denotes ordinary differentiation with respect to t. Dividing Eq. (4) by $\mathrm{X}(x)\mathrm{T}(t)$ leads to:

$$\frac{1}{D}\frac{\mathrm{T}(t)'}{\mathrm{T}(t)} = \frac{\mathcal{L}_\delta \mathrm{X}(x)}{\mathrm{X}(x)} \tag{5}$$

Since the left-hand side of Eq. (5) is a function of t only, and the right-hand side is a function of x only, we conclude that:

$$\frac{1}{D}\frac{\mathrm{T}(t)'}{\mathrm{T}(t)} = \frac{\mathcal{L}_\delta \mathrm{X}(x)}{\mathrm{X}(x)} = \text{constant in } x \text{ and } t = \psi^\delta \tag{6}$$

where the superscript δ in ψ^δ denotes the dependency on δ. As a result, a solution for the integro-differential equation (Eq. (1)) must be a solution to the following pair of equations, an ordinary differential equation (ODE) and an integral equation:

$$\mathrm{T}'(t) - D\psi^\delta \mathrm{T}(t) = 0 \tag{7}$$

$$\mathcal{L}_\delta \mathrm{X}(x) - \psi^\delta \mathrm{X}(x) = 0 \tag{8}$$

The general solution for the ODE (Eq. (7)) is:

$$\mathrm{T}(t) = \begin{cases} E & , \text{if } \psi^\delta = 0 \\ F\exp\left(D\psi^\delta t\right) & , \text{if } \psi^\delta \neq 0 \end{cases} \tag{9}$$

with E and F undetermined constants.

In the case of the integral equation (Eq. (8)), we search for a solution X with a form similar to that obtained when using separation of variables for the corresponding classical (local) diffusion PDE [22]. Then, ψ^δ is found by imposing that the integral equation (Eq. (8)) is satisfied for this X.

For this purpose, we briefly review the form of the solutions for the 1D linear classical diffusion equation, the local version of the nonlocal form in Eq. (1):

$$\frac{\partial u(x,t)}{\partial t} = D\nabla^2 u(x,t) \tag{10}$$

Separation of variables for Eq. (10) leads to:

$$\mathrm{T}^c(t) = \begin{cases} E & \psi^c = 0 \\ F\exp(D\psi^c t) & \psi^c \neq 0 \end{cases} \tag{11}$$

$$\mathrm{X}^c(x) = \begin{cases} Gx + H & \psi^c = 0 \\ I\sin kx + J\cos kx & \psi^c \neq 0 \end{cases} \tag{12}$$

where G, H, I, J, and k are undetermined constants, and $\psi^c = -k^2$ (see Appendix 1 and [22] for derivation details). The superscript c in T^c, X^c, and ψ^c stands for the "classical" solution.

We first show that $\mathrm{X}(x) = Gx + H$ satisfies Eq. (8) for $\psi^\delta = 0$. Indeed:

$$\begin{aligned} \mathcal{L}_\delta \mathrm{X}(x) &= \int_{\mathrm{H}_x} \mu\left(\left|\hat{x} - x\right|\right)\left[\mathrm{X}\left(\hat{x}\right) - \mathrm{X}(x)\right]\mathrm{d}\hat{x} \\ &= \int_{\mathrm{H}_x} \mu\left(\left|\hat{x} - x\right|\right) G\left(\hat{x} - x\right)\mathrm{d}\hat{x} \\ &= \int_{-\delta}^{\delta} \mu(|\xi|) G\xi \mathrm{d}\xi = 0 \end{aligned} \tag{13}$$

For nonzero ψ^δ, we assume the same form for the PD solution $\mathrm{X}(x)$ as that of the classical solution shown in Eq. (12):

$$\mathrm{X}(x) = I\sin kx + J\cos kx \tag{14}$$

We substitute Eq. (14) in Eq. (8) and solve for ψ^δ:

$$\begin{aligned} &\int_{\mathrm{H}_x} \mu\left(\left|\hat{x} - x\right|\right)\left[\left(I\sin k\hat{x} + J\cos k\hat{x}\right) - (I\sin kx + J\cos kx)\right]\mathrm{d}\hat{x} - \psi^\delta(I\sin kx + J\cos kx) = \\ &\int_{-\delta}^{\delta} \mu(|\xi|)[(I\sin k(x+\xi) + J\cos k(x+\xi)) - (I\sin kx + J\cos kx)]\mathrm{d}\xi - \psi^\delta(I\sin kx + J\cos kx) = \\ &(I\sin kx + J\cos kx)\left\{\int_{-\delta}^{\delta} \mu(|\xi|)\cos(k\xi)\mathrm{d}\xi - \int_{-\delta}^{\delta} \mu(|\xi|)\mathrm{d}\xi - \psi^\delta\right\} = 0 \end{aligned} \tag{15}$$

We introduce the following simplifying notations: $\beta^\delta = \int_{-\delta}^{\delta} \mu(|\xi|)\mathrm{d}\xi$, $\widehat{\mu}_k = \widehat{\mu}\left(\frac{Lk}{2\pi}\right) = \int_{-\infty}^{\infty} \mu(|\xi|)\cos(k\xi)\mathrm{d}\xi$. Observe that $\widehat{\mu}_k$ is the Fourier cosine transform of μ computed at $\frac{Lk}{2\pi}$. Then ψ^δ is obtained from Eq. (15) as:

$$\psi^\delta = \widehat{\mu}_k - \beta^\delta \tag{16}$$

As a result, we have the following forms for functions T and X for the PD solution:

$$\mathrm{T}(t) = \begin{cases} E & \psi^\delta = 0 \\ F\exp\left(D\psi^\delta t\right) & \psi^\delta \neq 0 \end{cases} \tag{17}$$

$$\mathrm{X}(x) = \begin{cases} Gx + H & \psi^\delta = 0 \\ I\sin kx + J\cos kx & \psi^\delta \neq 0 \end{cases} \tag{18}$$

We then write the "ansatz" solution of Eq. (1), $u(x,t)$, as a superposition of these functions for zero and nonzero ψ^δ:

$$u(x,t) = C_1 + C_2 x + \left(C_3\sin kx + C_4\cos kx\right)\exp\left(D\psi^\delta t\right) \tag{19}$$

where C_1,C_2, C_3, and C_4 are undetermined constants.

Similar to the procedure for classical PDEs [22], analytical solutions for specific linear PD diffusion initial and boundary value problems (IBVPs) can be obtained by applying first the boundary conditions and then the initial conditions to Eq. (19).

However, we observe that the formal solution in Eq. (19) is identical to the solution for the classical problem, which, from Eqs. (11) and (12), is:

$$u^c(x,t) = C_1 + C_2 x + \left(C_3\sin kx + C_4\cos kx\right)\exp\left(-Dk^2 t\right) \tag{20}$$

with the only difference being the replacement of the $\psi^c = -k^2$ factor with ψ^δ.

Therefore, by defining the *"peridynamic factor"* or the *"nonlocal factor"*:

$$A(k,\delta) = \frac{\psi^\delta}{\psi^c} = \frac{\beta^\delta - \widehat{\mu}_k}{k^2} \tag{21}$$

The *formal analytical solution of the peridynamic diffusion IBVP can be written directly from the solution of the corresponding classical (PDE-based) diffusion IBVP (Eq. (20)) by replacing $\psi^c = -k^2$ with $A(k,\delta)\psi^c$ in the time-exponential part of the solution.* Note that the further the PD factor is from value one, the stronger the nonlocal effect will be.

Remark 1: While in a classical BVP for a PDE, boundary conditions are used to define a well-posed problem; for nonlocal equations, conditions need to be defined over a "thick" region (of thickness δ) at the domain's frontier. These conditions are called nonlocal boundary conditions, or volume-constraints (see [23]). In many PD applications however, enforcing local boundary conditions is desired/needed since physical measurements are usually available only at the surface, not through a layer inside the body. Such conditions are described by local BCs. For these reasons, we will solve PD problems with associated local boundary conditions, and particular types of extending those local conditions over a fictitious layer of thickness equal to the horizon size, to generate corresponding nonlocal BCs or volume constraints. Various methods for applying local BCs to PD models have also been discussed in, for example, Aksoylu and Gazonas [24], D'Elia and Yu [25], Foss et al. [26], and Zhao et al. [27].

Remark 2: Given the convergence of PD solutions [28] to the classical solution as the nonlocality vanishes (δ goes to zero), one expects that a legitimate PD kernel function μ, satisfies $\lim_{\delta \to 0} A(k, \delta) = 1$ (see Eq. (21)).

In what follows, we present examples for finding the analytical solution for several PD IBVPs. We also study the properties of the nonlocal factor $A(k, \delta)$ for a class of kernels often used in PD applications. This includes the kernel obtained using a constructive approach (as shown in Chen and Bobaru [29] for diffusion problems, and Chen et al. [30] for elasticity), as well as two other types of PD kernels often used in the literature (see, e.g., [31–33].

3 Examples of Initial and Boundary Value Peridynamic Problems in 1D

First, we consider a nonlocal heat conduction IBVP (with Dirichlet boundary conditions) in a bar of length L, with given initial temperature $g(x)$ along the bar, and zero temperature imposed at the ends of the bar:

$$\begin{cases} \frac{\partial T(x,t)}{\partial t} = D\mathcal{L}_\delta T(x,t) \\ T(x,0) = g(x), 0 \le x \le L \\ T(0,t) = T(L,t) = 0, t > 0 \end{cases} \tag{22}$$

where $T(x,t)$ denotes the temperature at x and time t. We assume further that the kernel function (which specifies the PD Laplace operator) in this particular case has the form [29]:

$$\mu(|\xi|) = \begin{cases} \frac{(3-n)}{\delta^{(3-n)}} \frac{1}{|\xi|^n}, |\xi| \le \delta \\ 0, |\xi| > \delta \end{cases}, \text{with } n = 0, 1, \text{ or } 2. \tag{23}$$

In order to obtain the formal PD analytical solution for this problem, we first write the solution for the corresponding local problem:

$$\begin{cases} \frac{\partial T(x,t)}{\partial t} = D\nabla^2 T(x,t) \\ T(x,0) = g(x), 0 \le x \le L \\ T(0,t) = T(L,t) = 0, t > 0 \end{cases} \tag{24}$$

The exact solution to this local IBVP can be written as [34]:

$$T_c(x,t) = \sum_{m=1}^{\infty} B_m \sin k_m x \exp\left(-D{k_m}^2 t\right) \tag{25}$$

where $B_m = 2\int_0^L g(x) \sin k_m x \, \mathrm{d}x$, and $k_m = \frac{m\pi}{L}$ with m being a positive integer. Note that for other types of boundary conditions, the "wavenumber" k_m takes different forms (see Sects. 3.3 and 3.4).

The PD nonlocal factor for this case is:

$$\begin{aligned} A\left(k_m,\delta\right) &= \frac{-\psi^{\delta}}{k_m^2} = -\frac{\widehat{\mu}_{k_m}-\beta^{\delta}}{k_m^2} \\ &= -\frac{1}{k_m^2}\int_{-\delta}^{\delta}\frac{(3-n)}{\delta^{(3-n)}}\frac{1}{|\xi|^n}[\cos\left(k_m\xi\right)-1]\mathrm{d}\xi \\ &= -\frac{(3-n)}{\left(k_m\delta\right)^2}\int_{-1}^{1}\frac{\cos k_m\,\delta\xi-1}{|\xi|^n}\mathrm{d}\xi \end{aligned} \tag{26}$$

From Eq. (26), we observe that using kernels given by Eq. (23) leads to $A\left(k_m,\delta\right)=A_n\left(r_m\right)$ where $r_m=k_m\delta$, and the subscript n in A_n refers to the specific n value in the employed kernel. By replacing ${k_m}^2$ with $A_n\left(r_m\right){k_m}^2$ in the classical solution in Eq. (25), we arrive at:

$$T_{\mathrm{pd}}(x,t)=\sum_{m=1}^{\infty}B_m\,\sin k_m x\,\exp\left(-DA_n\left(r_m\right){k_m}^2 t\right) \tag{27}$$

The formula in Eq. (27) satisfies the PD problem in Eq. (22). Convergence of these PD series solutions is discussed in Appendix 2.

In what follows, we will focus on a few points related to convergence properties for the series solution and the nonlocal factor for the specific kernels shown in Eq. (23), assuming the necessary properties for initial and boundary conditions for calculations to be valid. In particular, we will investigate:

(a) Convergence to the classical solution when δ goes to zero, which is equivalent to showing that $A_n\left(r_m\right)$ converges to 1 when δ goes to zero, and.
(b) Satisfaction of the initial and boundary conditions.

We examine the points for different n values in Eq. (27). In particular, when $n=0$, we have

$$A_0\left(r_m\right)=-\frac{3}{{r_m}^2}\int_{-1}^{1}\left(\cos r_m\hat{x}-1\right)\mathrm{d}\hat{x}=\frac{6\left[1-\frac{\sin\left(r_m\right)}{r_m}\right]}{{r_m}^2} \tag{28}$$

When $n=1$, we have,

$$A_1\left(r_m\right)=-\frac{2}{{r_m}^2}\int_{-1}^{1}\frac{\cos r_m\hat{x}-1}{|\hat{x}|}\mathrm{d}\hat{x}=-\frac{4\left[\mathrm{Ci}\left(r_m\right)-\ln\left(r_m\right)-\gamma\right]}{{r_m}^2} \tag{29}$$

where Ci is the cosine integral function and $\mathrm{Ci}(x)=\gamma+\ln(x)+\int_0^x\frac{\cos z-1}{z}\mathrm{d}z$. γ is the Euler-Mascheroni constant, and

$$\gamma=\lim_{z\to 0}[\mathrm{Ci}(z)-\ln(z)]=\lim_{n\to\infty}\left(\left(\sum_{k=1}^{n}\frac{1}{k}\right)-\ln(n)\right)\approx 0.577215664901537 \tag{30}$$

When $n=2$, we have

$$A_2(r_m) = -\frac{1}{(r_m)^2}\int_{-1}^{1}\frac{\cos r_m\hat{x} - 1}{|\hat{x}|^2}\mathrm{d}\hat{x} = \frac{2\left[\mathrm{Si}(r_m) + \frac{\cos(r_m)-1}{r_m}\right]}{k_m\delta} \tag{31}$$

where Si is the sine integral function, and $\mathrm{Si}(x) = \int_0^x \frac{\sin z}{z}\mathrm{d}z$.

3.1 Pointwise Convergence to the Classical Solution when δ Goes to Zero

It is obvious that $A_0(r_m)$ converges to 1 when δ goes to zero for any m value, and that it converges to 0 when m goes to infinity for any $\delta > 0$. In Fig. 1, we plot the nonlocal factors for different $r_m = k_m\delta$ values. This figure reveals that, similar to $A_0(r_m)$, $A_1(r_m)$ and $A_2(r_m)$ also approach 1 when δ goes to zero, for any m value, and decay to 0 when m goes to infinity for any $\delta > 0$. As expected, Fig. 1 also shows that the PD formulation corresponding to the kernel with $n=0$ has a stronger nonlocal effect, while $n=2$ has the weakest, departing the least from the classical solution, because for a fixed r_m value, the nonlocal factor departs more from 1 when $n=0$ than when $n=2$.

To better understand the dependence of the nonlocal factor, $A_n(r_m)$, on m and δ, respectively, in Fig. 2, we plot the nonlocal factors with varying δ/L for different m values. This figure, again, shows that $A_n(r_m)$ values are between 0 and 1. In Fig. 3, we compare the nonlocal factors $A_0(r_m)$, $A_1(r_m)$, and $A_2(r_m)$. The further these factors are from value one, the stronger the nonlocal effect.

3.2 Initial and Boundary Conditions

Note that when $t=0$, this solution is the same as the classical solution, so the PD solution for $t=0$ matches the given initial condition.

The imposition of local boundary conditions in PD can take different forms. For example, to impose the local Dirichlet boundary condition (see Eq. (22)) in the PD model, three possible options are shown in Fig. 4: mirror-type (temperature field in the nonlocal boundary domain is related by mirror symmetry to the corresponding domain in the bar, see Fig. 4A), naïve-type (temperature field in the nonlocal boundary layer is

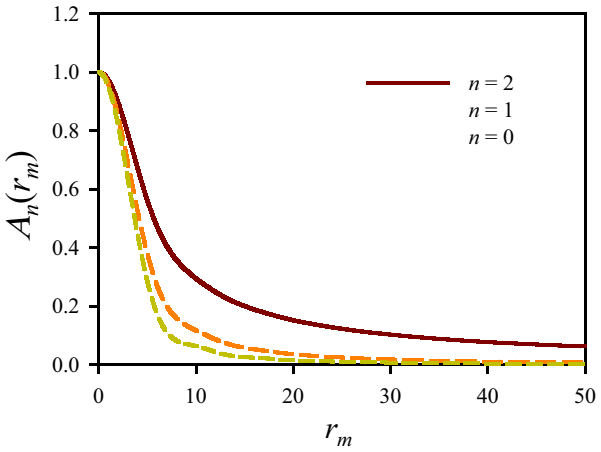

Fig. 1 The nonlocal factor versus parameter r_m, for different peridynamic kernels

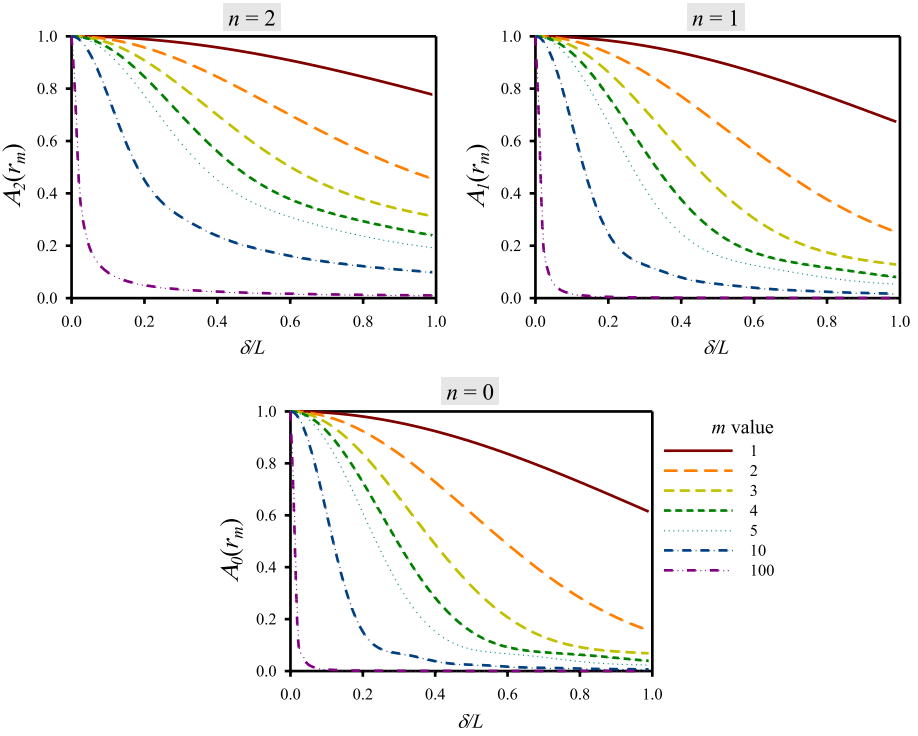

Fig. 2 The nonlocal factor (for various terms (m) in the series) versus the normalized nonlocal size δ/L, for different types of peridynamic kernels

constant and equal to the value of the local Dirichlet condition, see Fig. 4B), and inner-type (temperature field in a finite layer inside the domain is fixed to be the local boundary temperature, see Fig. 4C). Rigorous descriptions for imposing various local BCs into nonlocal models are described in, for example, [24, 35–37].

Fig. 3 The nonlocal factor for different peridynamic kernels as a function of horizon size, for different terms m in the series

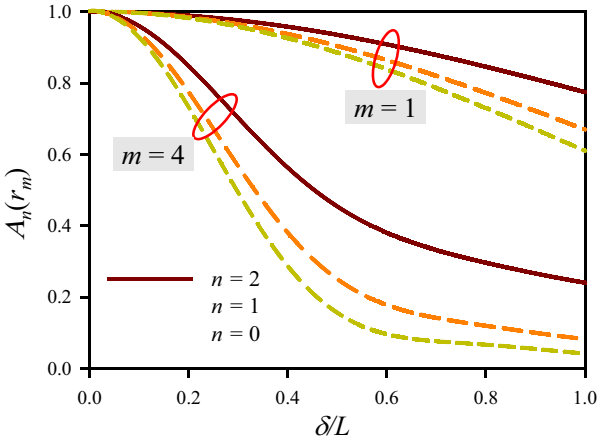

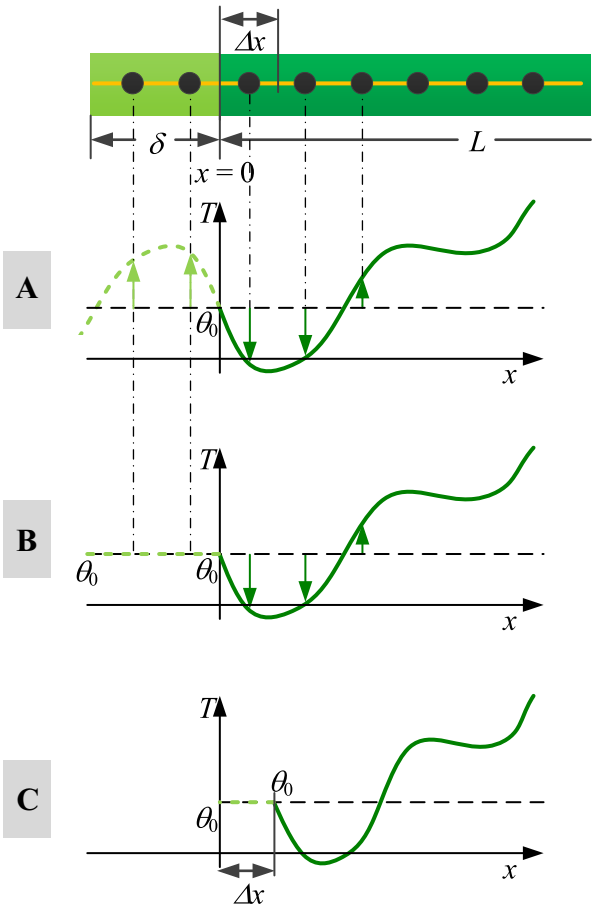

Fig. 4 Three types of imposing Dirichlet boundary conditions in a 1D PD model: **A** mirror-type, **B** naïve-type, and **C** inner-type

While there is a single problem defined by the PD equation and the local boundary conditions we aim to enforce, the different implementations of such conditions mentioned in Fig. 4 correspond, in general, to slightly different nonlocal problems: the PD equation and different associated nonlocal boundary conditions (or "volume constraints"). The formal solution obtained in Eq. (27), is just a particular way to satisfy the imposed initial and local boundary conditions. We now observe the behavior of the PD analytical solution for the problem defined by Eq. (22) in the nonlocal layer normally associated with the volume constraints of a nonlocal problem.

On the left side boundary of the 1D bar, we have (see Eq. (24)):

$$T_{\mathrm{pd}}(-x,t) = \sum_{m=1}^{\infty} B_m \sin k_m(-x)\exp\left(-DA_n\left(r_m\right){k_m}^2 t\right) = -T_{\mathrm{pd}}(x,t) \tag{32}$$

and,

$$T_{\mathrm{pd}}(0,t) = 0 \tag{33}$$

On the right side, since $2Lk_m = 2m\pi$, we have:

$$T_{\text{pd}}(2L - x, t) = \sum_{m=1}^{\infty} B_m \sin k_m(2L - x)\exp\left(-DA_n\left(r_m\right){k_m}^2 t\right) = -T_{\text{pd}}(x, t) \tag{34}$$

and,

$$T_{\text{pd}}(L, t) = 0 \tag{35}$$

Therefore, the Dirichlet boundary conditions are automatically satisfied, and the nonlocal boundary conditions are of the mirror-type.

Note that the constant profile for the influence function that defines the kernel is only one option, and other profiles are possible [29, 38]. In this paper, we focus on the constant profile only, and describe the formal, simple way to construct analytical peridynamic solutions similar to the way series solutions are built using the separation of variables method for classical PDEs. For other choices of the influence function profile, one can follow the same procedure to construct formal solutions and check if the solution satisfies the initial and boundary conditions. We also note that the approach discussed so far works only for a constant horizon size used over the domain. If the horizon size changes over the domain, then the nonlocal factor depends on location as well and separation of variables approach may no longer work.

We apply this strategy of constructing analytical solutions to PD equations for transient diffusion problems with local boundary conditions in the examples below. The first example has Dirichlet boundary conditions, while the second one has Dirichlet–Neumann boundary conditions. For the first case, we give the detailed results for the $n=2$ selection, but also compare with results from $n=0$ and $n=1$. For the second case, we only show results for the PD formulation with a kernel that uses $n=2$.

3.3 Example 1: Solution for a 1D Diffusion Problem with Dirichlet Boundary Conditions

Consider a rod of length $L=10$ cm with an initial temperature 100 °C. The left and right sides of this rod are maintained at a temperature of 0 °C. The thermal diffusivity is $D=1.14$ cm^2/s. Using these values in Eq. (27), we obtain the analytical PD solution as follows:

$$T_{\text{pd}}(x, t) = \sum_{m=1,3,5\ldots}^{\infty} \frac{4\theta_o}{m\pi} \sin k_m x \exp\left(-DA_n\left(r_m\right){k_m}^2 t\right) \tag{36}$$

where $\theta_o = 100$ °C.

Figure 5 shows the temperature profiles at three different times for the $n = 2$ case. Four different horizon sizes are considered for the PD solution. The first 100 terms of the PD series solution are used for this plot. The classical solution is treated as a special case (horizon equal to zero) of the peridynamic solutions. Figure 5 reveals that even for a horizon size-bar length ratio of 0.2, the PD analytical solution is close to the classical solution. Initially, there are heat flux singularities at the ends of the bar. These singularities disappear instantly since the classical solution at any time after the initial time is infinitely smooth. For a larger horizon size, for instance, $0.2L$, the sharp gradient close to the left end is "averaged" over a larger domain. This explains the relative large difference at time $t=0.1$ s.

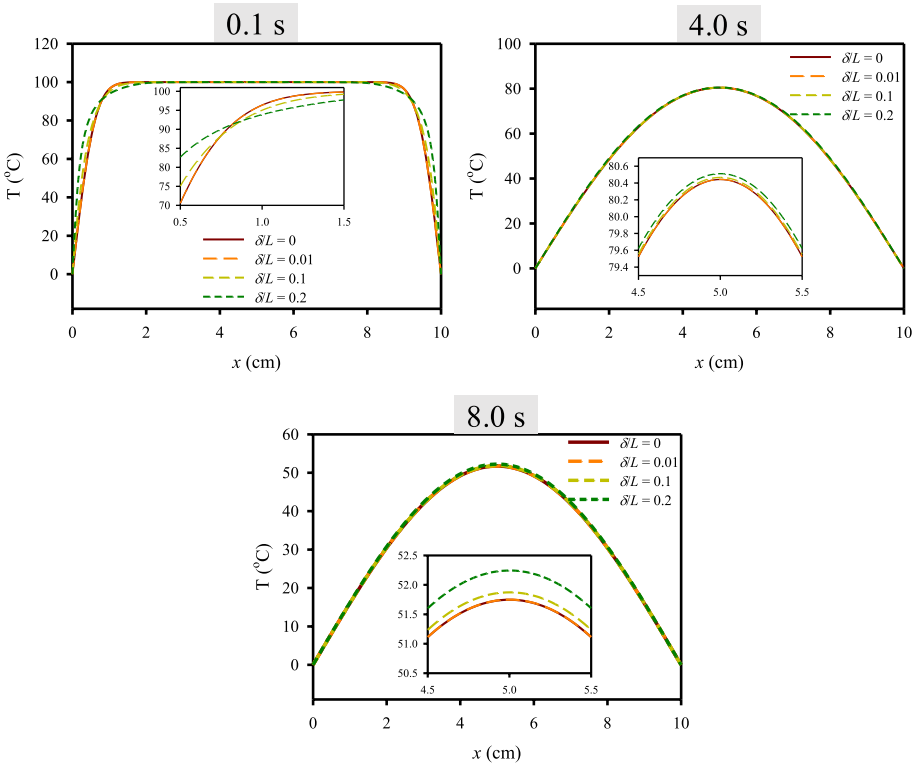

Fig. 5 Example 1: temperature profiles at time $t=0.1$ s, $t=4.0$ s, and $t=8.0$ s, from analytical PD solutions (for $n=2$) with four different ratios between the horizon sizes and the bar length: 0, 0.01, 0.1, and 0.2

Figure 6 compares the temperature profiles at three different times for PD formulations with different n values. Due to the symmetry of the solutions, only half of their profiles (x ranging from 0 to 5 cm) are shown in these plots. Similar to what we saw in Fig. 1, the PD formulation corresponding to the kernel with $n=0$ has a stronger nonlocal effect compared with the other two; the one with $n=2$, has the weakest nonlocal effect.

An interesting observation about the solution curve at $t=0.1$ s corresponding to $n=0$, is that the solution appears to be piecewise linear, and the extent of each linear piece is the same as the length of the horizon size. As time progresses, smoothness of the nonlocal temperature profile increases (see Fig. 6). Moreover, the ratio between the exponential function in any term with $m>1$ in Eq. (36) and the term with $m=1$ decays exponentially in time. Therefore, the nonlocal effect is expected to decay in time, meaning that the nonlocal analytical solution gets closer and closer to the exact classical solution as time marches on. We shall see in part II of this work [21] that this property is characteristic only to diffusion processes, and that in elastic wave propagation problems, nonlocality's influence does not necessarily decrease in time.

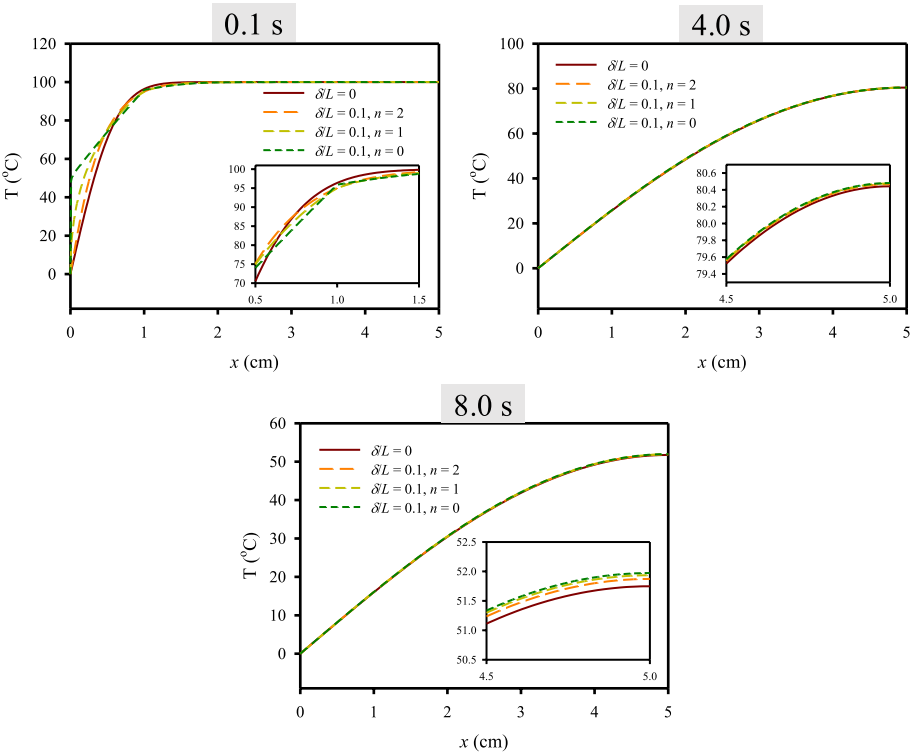

Fig. 6 Example 1: comparison, in time, of the solutions from PD formulations with different kernel (different n values)

3.4 Example 2: Solution for a 1D Diffusion Problem with Dirichlet and Neumann Boundary Conditions

Consider a rod of length $L = \pi$ cm with an initial temperature 0 °C [39]. The left side of this rod is maintained at a temperature of 20 °C. At the right end, a heat-flux -3 WD/cm^2 is imposed (D is the thermal diffusivity). The thermal diffusivity is $D = 1.14$ cm^2/s. With the classical solution available from Bobaru and Duangpanya [39], according to our discussion in the beginning of Sect. 3, the analytical PD solution is:

$$T_{\text{pd}}(x,t) = 20 + 3x + \sum_{m=1,3,5\ldots}^{\infty} C_m \sin k_m x \exp\left(-DA_n\left(r_m\right){k_m}^2 t\right) \tag{37}$$

where, given the Dirichlet–Neumann boundary conditions, $k_m = \frac{m\pi}{2L}$.

$$C_m = \frac{2}{L}\left(\frac{40+6L}{m}\cos\frac{mL}{2} - \frac{12}{m^2}\sin\frac{mL}{2} - \frac{40}{m}\right) \tag{38}$$

Note that the nonlocal factor $A_n\left(r_m\right)$ is different from the one with Dirichlet-Dirichlet boundary conditions, since k_m is different. We check to see if the boundary conditions are satisfied. On the left side boundary (Dirichlet conditions), we have:

$$T_{\mathrm{pd}}(-x,t)-20=-3x-\sum_{m=1,3,5\ldots}^{\infty}C_m\,\sin k_m x\,\exp\left(-DA_n\left(r_m\right){k_m}^2t\right)=20-T_{\mathrm{pd}}(x,t) \tag{39}$$

and,

$$T_{\mathrm{pd}}(0,t)=20 \tag{40}$$

On the right side boundary, we have a Neumann condition. To check this, we compute the spatial derivative:

$$\frac{\partial T_{\mathrm{pd}}(x,t)}{\partial x}=3+\sum_{m=1,3,5\ldots}^{\infty}k_m\,C_m\cos k_m x\,\exp\left(-DA_n\left(r_m\right){k_m}^2t\right) \tag{41}$$

Then:

$$\left.\frac{\partial T_{\mathrm{pd}}(x,t)}{\partial x}\right|_{2L-x}-3=-\sum_{m=1,3,5\ldots}^{\infty}k_m\,C_m\cos k_m x\,\exp\left(-DA_n\left(r_m\right){k_m}^2t\right)=3-\left.\frac{\partial T_{\mathrm{pd}}(x,t)}{\partial x}\right|_{x} \tag{42}$$

and,

$$\left.\frac{\partial T_{\mathrm{pd}}(x,t)}{\partial x}\right|_{x=L}=3 \tag{43}$$

This shows that the PD analytical solution satisfies the given local Dirichlet and Neumann boundary conditions.

Figure 7 shows the temperature profiles at three different times, for this heat transient diffusion problem with Dirichlet–Neumann boundary condition. Only the PD formulation with $n=2$ is considered in this case. Four different horizon sizes are considered. The classical solution is treated as a limiting case of the peridynamic solutions (by substituting $r_m=0$ into Eq. (37)). Figure 7 reveals that even with horizon size to bar-length ratio of 0.4, the PD analytical solution is close to the classical solution. Initially, there is a heat flux singularity at the left end of the bar. The singularity disappears instantly since the classical solution at any time after the initial time is infinitely smooth.

4 Analytical Solutions for 2D Transient Peridynamic Diffusion

In this section, we extend the approach introduced in the previous sections to construct analytical PD solutions for 2D transient heat/mass transfer. Extensions to 3D problems would follow a similar pathway.

The linear PD transient diffusion equation in 2D (or 3D) can be expressed as:

$$\frac{\partial u(\boldsymbol{x},t)}{\partial t}=D\mathcal{L}_\delta u(\boldsymbol{x},t) \tag{44}$$

where the PD Laplacian operator:

$$\mathcal{L}_\delta u(\boldsymbol{x},t)=\int_{\mathrm{H}_x}\mu\left(\left|\hat{\boldsymbol{x}}-\boldsymbol{x}\right|\right)\left[u\left(\hat{\boldsymbol{x}},t\right)-u(\boldsymbol{x},t)\right]\mathrm{d}V_{\hat{\boldsymbol{x}}} \tag{45}$$

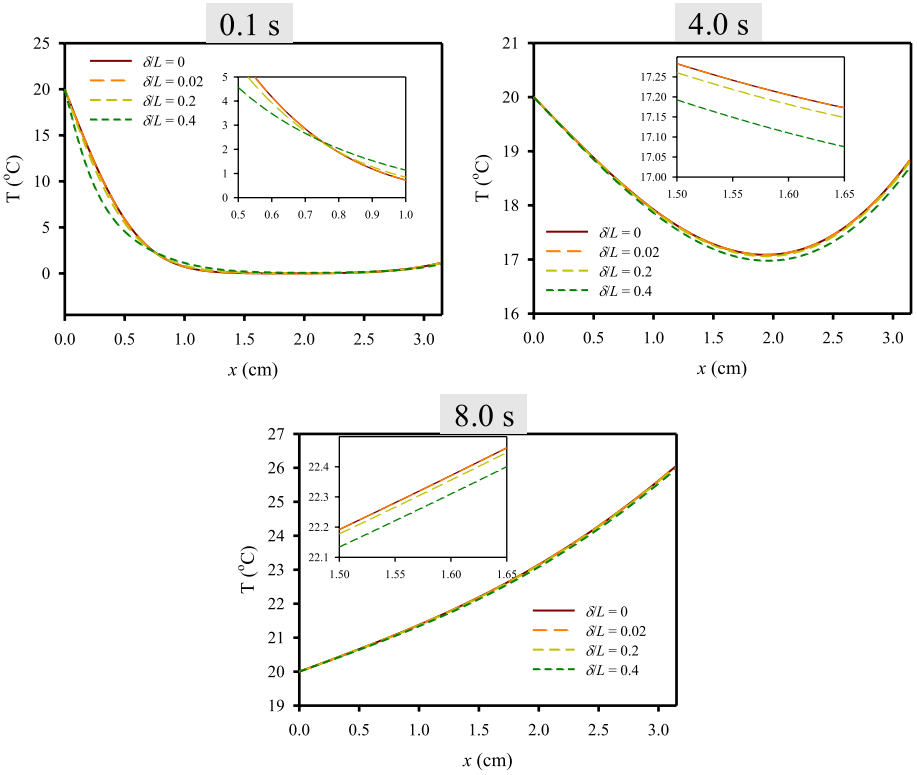

Fig. 7 Example 2: temperature profiles at times $t=0.1$ s, 4.0 s, and 8.0 s, from PD analytical solutions ($n=2$) with four different ratios between the horizon sizes and the bar length: 0, 0.02, 0.2, and 0.4

is the area/volume integral over H_x. Boldfaced letters denote vector-valued quantities, e.g., $\boldsymbol{x} = \left\{ \begin{array}{c} x \\ y \end{array} \right\}$ is the position vector in 2D**.** The neighborhood $\mathrm{H}_{\boldsymbol{x}}$ in 2D, is a disk centered at $\boldsymbol{x}$ with the radius δ. $\mathrm{d}V_{\hat{\boldsymbol{x}}}$ is the volume of node $\hat{\boldsymbol{x}}$ covered by the horizon of node $\boldsymbol{x}$. μ is the *kernel* function with $\mu = \mu(|\boldsymbol{\xi}|)$, that has the support $\mathrm{H}_{\boldsymbol{x}}$, therefore $\mu(|\boldsymbol{\xi}|) = 0$ for $|\boldsymbol{\xi}| > \delta$, where $\boldsymbol{\xi} = \hat{\boldsymbol{x}} - \boldsymbol{x}$ is the bond vector.

Following the method of separation of variables in 2D, we seek a solution in the following form:

$$u(x, y, t) = \mathrm{S}(x, y)\mathrm{T}(t) = \mathrm{X}(x)\mathrm{Y}(y)\mathrm{T}(t) \tag{46}$$

Substituting Eq. (46) into Eq. (44) gives:

$$\mathrm{S}(x, y)\mathrm{T}'(t) = D\mathrm{T}(t)\mathcal{L}_\delta \mathrm{S}(x, y) \tag{47}$$

and dividing Eq. (47) by ST yields:

$$\frac{1}{D}\frac{\mathrm{T}'(t)}{\mathrm{T}(t)} = \frac{\mathcal{L}_\delta \mathrm{S}(x, y)}{\mathrm{S}(x, y)} = \text{constant in } x,\ y,\ t \text{ (depends on } \delta) = \psi^\delta \tag{48}$$

As a result, the solution to the integro-differential equation Eq. (44) is the solution to the following pair of equations, an ODE and an integral equation:

$$\mathrm{T}'(t) - D\psi^{\delta}\mathrm{T}(t) = 0 \tag{49}$$

$$\mathcal{L}_{\delta}\mathrm{S}(x,y) - \psi^{\delta}\mathrm{S}(x,y) = 0 \tag{50}$$

The ODE in Eq. (49) is identical to that from the 1D case, yielding solution for T as given in Eq. (27).

For the integral equation Eq. (50), we choose $\mathrm{S}(x,y)$ to be the same as the spatial solutions obtained when using separation of variables for the corresponding classical (local) diffusion PDE (see Appendix 1). Then ψ^{δ} is found from requiring that Eq. (50) is satisfied for this $\mathrm{S}(x,y)$.

For the 2D classical diffusion equation, separation of variables leads to the following formal solutions (see Appendix 1):

$$\mathrm{T}^{c}(t) = \begin{cases} a_1 & \psi^{c} = 0 \\ a_2\exp(D\psi^{c}t) & \psi^{c} \neq 0 \end{cases} \tag{51}$$

$$\mathrm{S}^{c}(x,y) = \mathrm{X}^{c}(x)\mathrm{Y}^{c}(y) = \begin{cases} (a_3 + a_4x)(a_5 + a_6y) & \psi^{c} = 0 \\ (a_7\sin k_1x + a_8\cos k_1x)(a_9\sin k_2y + a_{10}\cos k_2y) & \psi^{c} \neq 0 \;\&\; k_1 \neq 0 \;\&\; k_2 \neq 0 \\ (a_5 + a_6y)(a_7\sin k_1x + a_8\cos k_1x) & \psi^{c} \neq 0 \;\&\; k_1 \neq 0 \;\&\; k_2 = 0 \\ (a_3 + a_4x)(a_9\sin k_2y + a_{10}\cos k_2y) & \psi^{c} \neq 0 \;\&\; k_1 = 0 \;\&\; k_2 \neq 0 \end{cases} \tag{52}$$

where $a_1, a_2, \ldots, a_{10}$, and k_1 and k_2 are constants, and $\psi^{c} = -\left(k_1^2 + k_2^2\right)$.

We first show that $\mathrm{S}(x,y) = \left(a_3 + a_4x\right)\left(a_5 + a_6y\right)$ satisfies the integral Eq. (50) for $\psi^{\delta} = 0$:

$$\begin{aligned}
\mathcal{L}_{\delta}\mathrm{S}(x,y) &= \int_{\mathrm{H}_x} \mu\left(\left|\hat{\boldsymbol{x}} - \boldsymbol{x}\right|\right)\left[(a_3 + a_4\hat{x})(a_5 + a_6\hat{y}) - (a_3 + a_4x)(a_5 + a_6y)\right]\mathrm{d}\hat{x}\mathrm{d}\hat{y} \\
&= \int_{\mathrm{H}_x} \mu\left(\left|\hat{\boldsymbol{x}} - \boldsymbol{x}\right|\right)\left[a_4a_5\hat{x} + a_3a_6\hat{y} + a_4a_6\hat{x}\hat{y} - a_4a_5x - a_3a_6y - a_4a_6xy\right]\mathrm{d}\hat{x}\mathrm{d}\hat{y} \\
&= \int_0^{2\pi}\int_0^{\delta} \mu(R)\left[a_4a_5(R\cos\varphi) + a_3a_6(R\sin\varphi)\right. \\
&\quad \left. + a_4a_6\left(xR\sin\varphi + yR\cos\varphi + R^2\sin\varphi\cos\varphi\right)\right]R\mathrm{d}R\mathrm{d}\varphi = 0
\end{aligned} \tag{53}$$

In the case of $\psi^{\delta} \neq 0$, one can show that all of the corresponding $\mathrm{S}(x,y)$ terms in Eq. (52) satisfy the PD integral (Eq. (50)) only if:

$$\begin{aligned}
\psi^{\delta} &= \int_0^{2\pi}\int_0^{\delta} \mu(R)\left[\cos\left(k_1\,R\cos\varphi\right)\cos\left(k_2\,R\sin\varphi\right) - 1\right]R\mathrm{d}R\mathrm{d}\varphi = 2\pi\frac{\delta^2}{r^2}\int_0^{r} \mu\left(\frac{\delta R}{r}\right)R\left[J_0(R) - 1\right]\mathrm{d}R \\
&= 2\pi\int_0^{\delta} \mu(w)w\left[J_0\left(\sqrt{k_1^2 + k_2^2}w\right) - 1\right]\mathrm{d}w = 2\pi\hat{\mu}_{\boldsymbol{k}} - \beta^{\delta}
\end{aligned} \tag{54}$$

where $r = \sqrt{\left(k_1\delta\right)^2 + \left(k_2\delta\right)^2} = \delta\sqrt{-\psi^c}$, J_0 is the zeroth-order Bessel function of the first kind, and therefore, $\widehat{\mu}_{\boldsymbol{k}} = \int_0^\infty \mu(w) w J_0\left(\sqrt{k_1^2 + k_2^2}\, w\right) \mathrm{d}w$ is the Hankel transform of order zero for μ evaluated at $\sqrt{k_1^2 + k_2^2} = \sqrt{-\psi^c}$, and $\beta^\delta = \int_0^{2\pi}\int_0^\delta \mu(w) w \mathrm{d}w\mathrm{d}\varphi$ is the integral of the kernel function. Note that for radially symmetric function such as μ, Hankel transform of order zero is equivalent to the 2D Fourier transform [40]. As a result, ψ^δ has a similar relationship with μ in 2D as it does in 1D (see Eq. (16)). Details for the derivation of Eq. (54) are given in Appendix 3.

For conciseness, we only show that the terms in Eq. (52) satisfy the PD integral (Eq. (50)) for one of them. The process for the rest of the terms is similar. Let $\mathrm{S}(x, y) = \sin k_1 x \sin k_2 y$, then:

$$
\begin{aligned}
\mathcal{L}_\delta\left(\sin k_1 x \sin k_2 y\right) &= \int_{\mathrm{H}_x} \mu\left(|\hat{\boldsymbol{x}} - \boldsymbol{x}|\right)\left(\sin k_1\hat{x} \sin k_2\hat{y} - \sin k_1 x \sin k_2 y\right)\mathrm{d}\hat{x}\mathrm{d}\hat{y} \\
&- \psi^\delta \sin k_1 x \sin k_2 y = \int_0^{2\pi}\int_0^\delta \mu(R)\left[\sin\left(k_1 x + k_1 R\cos\varphi\right)\right. \\
&\left.\sin\left(k_2 y + k_2 R\sin\varphi\right) - \sin k_1 x \sin k_2 y\right] R\mathrm{d}R\mathrm{d}\varphi \\
&- \psi^\delta \sin k_1 x \sin k_2 y = \int_0^{2\pi}\int_0^\delta \mu(R) \\
&\left\{\sin k_1 x \sin k_2 y\left[\cos\left(k_1 R\cos\varphi\right)\cos\left(k_2 R\sin\varphi\right) - 1\right]\right. \\
&+\sin k_1 x \cos k_2 y \cos\left(k_1 R\cos\varphi\right)\sin\left(k_2 R\sin\varphi\right) \\
&+\cos k_1 x \sin k_2 y \sin\left(k_1 R\cos\varphi\right)\cos\left(k_2 R\sin\varphi\right) \\
&\left.+\cos k_1 x \cos k_2 y \sin\left(k_1 R\cos\varphi\right)\sin\left(k_2 R\sin\varphi\right)\right\} R\mathrm{d}R\mathrm{d}\varphi \\
&- \psi^\delta \sin k_1 x \sin k_2 y = \sin k_1 x \sin k_2 y \\
&\left\{\int_0^{2\pi}\int_0^\delta \mu(R)\left[\cos\left(k_1 R\cos\varphi\right)\cos\left(k_2 R\sin\varphi\right) - 1\right] R\mathrm{d}R\mathrm{d}\varphi - \psi^\delta\right\} = 0
\end{aligned}
\tag{55}
$$

which gives ψ^δ as expressed in Eq. (54).The PD nonlocal factor for 2D transient diffusion is then:

$$
A\left(k_1, k_2, \delta\right) = \frac{\psi^\delta}{\psi^c} = \frac{2\pi\widehat{\mu}_{\boldsymbol{k}} - \beta^\delta}{-\left(k_1^2 + k_2^2\right)} = -2\pi\frac{\delta^4}{r^4}\int_0^r \mu\left(\frac{\delta R}{r}\right) R\left[J_0(R) - 1\right]\mathrm{d}R \tag{56}
$$

One can therefore *find the analytical solution for a 2D peridynamic (nonlocal) diffusion IBVP by directly using the analytical solution for the corresponding 2D classical (PDE-based) diffusion IBVP and* replacing $\psi^c = -\left(k_1^2 + k_2^2\right)$ with $A\left(k_1, k_2, \delta\right)\psi^c$ in the time-exponential part of the solution. A similar analysis can be carried out for 3D problems.

Next, we present an example for finding analytical solutions to a 2D PD IBVP with Dirichlet and Neumann BCs and also study the properties of the nonlocal factor $A\left(k_1, k_2, \delta\right)$ in 2D for the class of singular kernels most commonly used in PD modeling.

5 Example of the Analytical Solution for an Initial Boundary Value Peridynamic Problem in 2D

We consider peridynamic diffusion in 2D with mixed Dirichlet–Neumann boundary conditions in a rectangular domain of length L and height H. The equation and corresponding Dirichlet and Neumann BCs are:

$$\begin{cases} \frac{\partial T(x,y,t)}{\partial t} = D\mathcal{L}_\delta T(x,y,t) \\ T(0,y,t) = T(L,y,t) = 0 \\ T(x,0,t) = 0; \frac{\partial T(x,y,t)}{\partial y}\Big|_{y=H} = 0 \\ T(x,y,0) = f(x,y) \end{cases} \tag{57}$$

with the kernel function that specifies the PD Laplacian operator to be of the form:

$$\mu(|\xi|) = \begin{cases} \frac{2(4-n)}{\pi\delta^{(4-n)}}\frac{1}{|\xi|^n}, & |\xi| \le \delta \\ 0, & |\xi| > \delta \end{cases}, \text{and } n = 0, 1, 2 \tag{58}$$

where the kernel function with $n=2$ was given in Bobaru and Duangpanya [41]. The kernel functions with $n=0$, 1 are derived by following the same derivation process shown in Bobaru and Duangpanya [41]: equating the PD flux to the classical flux through a surface arising from a linear temperature profile.

To obtain the solution, we first find the solution to the classical diffusion equation subjected to the same boundary and initial conditions. This is (see [34]):

$$T_c(x,y,t) = \sum_{s=1}^{\infty}\sum_{m=1}^{\infty} B_{ms}\,\sin\left(k_m x\right)\,\sin\left(k_s y\right)\,\exp\left(-\left({k_m}^2 + {k_s}^2\right)Dt\right) \tag{59}$$

where,

$$B_{ms} = \frac{4}{LH}\int_0^L\int_0^H f(x,y)\sin\left(k_m x\right)\sin\left(k_s y\right)\mathrm{d}y\mathrm{d}x \tag{60}$$

The "wavenumbers" in this 2D case are $k_m = \frac{m\pi}{L}$, and $k_s = \frac{\left(s-\frac{1}{2}\right)\pi}{H}$, where m and s are positive integers.

We then compute the PD nonlocal factor from Eq. (56) for the kernel type in Eq. (58):

$$\begin{aligned} A_n\left(k_m, k_s, \delta\right) &= -2\pi\frac{\delta^4}{r^4}\frac{2(4-n)}{\pi\delta^{(4-n)}}\int_0^r \frac{1}{\left(\frac{\delta R}{r}\right)^n} R\left[J_0(R) - 1\right]\mathrm{d}R \\ &= -\frac{4(4-n)}{r^{(4-n)}}\int_0^r \frac{J_0(R)-1}{R^{n-1}}\mathrm{d}R \end{aligned} \tag{61}$$

where $r = r(m,s) = \sqrt{\left(k_m\delta\right)^2 + \left(k_s\delta\right)^2}$, and J_0 is the zeroth-order Bessel function of the first kind. Similar to the 1D case, we observe that with the kernels of the form in Eq. (58), the PD analytical solution is obtained from the classical solution by replacing $-\left({k_m}^2 + {k_s}^2\right)$ with $-A_n\left(k_m, k_s, \delta\right)\left({k_m}^2 + {k_s}^2\right)$:

$$T_{\mathrm{pd}}(x,y,t)=\sum_{s=1}^{\infty}\sum_{m=1}^{\infty}B_{ms}\,\sin\left(k_m x\right)\sin\left(k_s y\right)\exp\left(-\left({k_m}^2+{k_s}^2\right)A_n\left(k_m,k_s,\delta\right)Dt\right) \tag{62}$$

5.1 Convergence to the Classical Solution and PD Boundary Conditions

In this section, we check the pointwise convergence behavior of the formula in Eq. (62) and whether it satisfies the initial and boundary conditions.

Since $\cos\left(k_m\delta\widehat{x}\right)\cos\left(k_s\delta\widehat{y}\right)-1\le 0$(see Eq. (55)), for the kernel type in Eq. (58), $A_n\left(k_m,k_s,\delta\right)=A_n(r)>0$. Therefore, the exponential functions in Eq. (62) are between 0 and 1, for any $t\ge 0$. Since Eq. (62) converges when the exponential functions are 0 or 1, the 2D PD solution converges.

With $n=0$, 1 and 2 substituted in Eq. (61), we obtain:

$$A_n(r)=\begin{cases}\frac{8}{r^3}\left(r-2J_1(r)\right), & n=0\\ \frac{12}{r^2}\left(1-{}_1F_2\left(\frac{1}{2};1,\frac{3}{2};-\frac{r^2}{4}\right)\right), & n=1\\ {}_2F_3\left(1,1;2,2,2;-\frac{r^2}{4}\right), & n=2\end{cases} \tag{63}$$

where J_1 is the first-order Bessel function of the first kind,${}_1F_2$ and ${}_2F_3$ are hypergeometric functions [42].

In the following, we check whether the solution converges to the classical solution when δ goes to zero ($A_n(r)$ needs to converge to 1 when δ or r goes to zero). In Fig. 8, we plot the nonlocal factors for various r values. The results show that $A_n(r)$ converge to 1 when r goes to zero (δ goes to zero for any m and s.), and converge to 0 when r goes to infinity (m *or* s goes to infinity for any none zero δ). Figure 8 also indicates that the PD formulation corresponding to the kernel with $n=0$, has a larger nonlocal effect compared to the other two, and the one with $n=2$, has the smallest nonlocal effect.

For the analytical solutions in the form of infinite series (Eq. (62)), the terms with the small (m, s) values dominate, especially when time t gets larger. In Fig. 9, we plot the nonlocal factors versus normalized horizon size, for three pairs of small m and s values. The

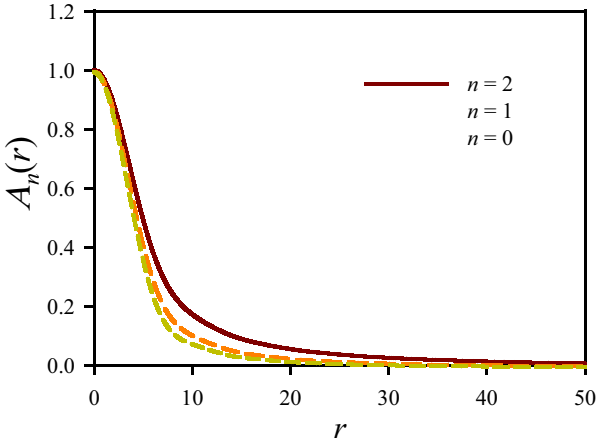

Fig. 8 Comparison of the 2D nonlocal factors for different peridynamic kernels. $r=\sqrt{\left(k_m\delta\right)^2+\left(k_s\delta\right)^2}$

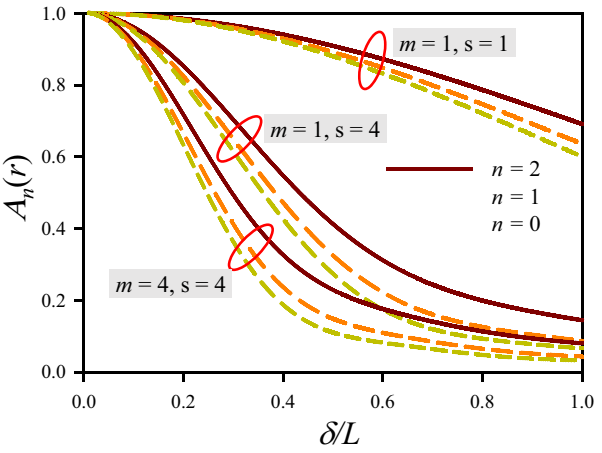

Fig. 9 The nonlocal factors versus normalized horizon size, for three pairs of relatively small m and s values: $m=1$, $s=1$; $m=1$, $s=4$; $m=4$, $s=4$

term corresponding to the smallest m and s values has the lowest nonlocal effect. When time t gets larger, the ratio between the exponential function in the first term ($m=1$, $s=1$) of Eq. (62) and the one in any other term ($m \neq 1$, $s \neq 1$) grows exponentially. Therefore, the nonlocal effect is expected to decay during the heat transient diffusion process. A similar conclusion was noticed in the 1D case (see Sect. 3.4).

When $t=0$, the PD solution is the same as the classical solution for any horizon size, and the initial condition ($T(x,y,0)=f(x,y)$) is automatically satisfied. We now check the PD boundary conditions.

At the boundary $x=0$, we have:

$$T(0,y,t)=0 \tag{64}$$

$$T(-x,y,t)=\sum_{s=1}^{\infty}\sum_{m=1}^{\infty}B_{ms}\sin\left(-k_m x\right)\sin\left(k_s y\right)\exp\left(-\left(k_m{}^2+k_s{}^2\right)A_n(r)Dt\right)=-T(x,y,t) \tag{65}$$

At the boundary $x=L$, we have:

$$T(L,y,t)=0 \tag{66}$$

$$T(2L-x,y,t)=\sum_{s=1}^{\infty}\sum_{m=1}^{\infty}B_{ms}\sin\left(\frac{m\pi}{L}(2L-x)\right)\sin\left(k_s y\right)\exp\left(-\left(k_m{}^2+k_s{}^2\right)A_n(r)Dt\right)=-T(x,y,t) \tag{67}$$

At the boundary $y=0$, we have:

$$T(x,0,t)=0 \tag{68}$$

$$T(x,-y,t)=\sum_{s=1}^{\infty}\sum_{m=1}^{\infty}B_{ms}\sin\left(k_m x\right)\sin\left(-k_s y\right)\exp\left(-\left(k_m{}^2+k_s{}^2\right)A_n(r)Dt\right)=-T(x,y,t) \tag{69}$$

At the boundary $y=H$, we have a Neumann boundary condition. We compute the corresponding partial derivative:

$$\frac{\partial T(x,y,t)}{\partial y} = \sum_{s=1}^{\infty}\sum_{m=1}^{\infty} k_s B_{ms} \sin\left(k_m x\right)\cos\left(k_s y\right)\exp\left(-\left({k_m}^2 + {k_s}^2\right)A_n(r)Dt\right) \tag{70}$$

When $y = H$, we get:

$$\left.\frac{\partial T(x,y,t)}{\partial y}\right|_{y=H} = 0 \tag{71}$$

$$\begin{aligned}\left.\frac{\partial T(x,y,t)}{\partial y}\right|_{2H-y} &= \sum_{s=1}^{\infty}\sum_{m=1}^{\infty} k_s\, B_{ms}\, \sin\left(k_m x\right)\cos\left(\frac{\left(s-\frac{1}{2}\right)\pi}{H}(2H-y)\right)\exp\left(-\left({k_m}^2 + {k_s}^2\right)A_n(r)Dt\right)\\ &= \sum_{s=1}^{\infty}\sum_{m=1}^{\infty} k_s\, B_{ms}\, \sin\left(k_m x\right)\cos\left((2s-1)\pi - k_s y\right)\exp\left(-\left({k_m}^2 + {k_s}^2\right)A_n(r)Dt\right)\\ &= -\sum_{s=1}^{\infty}\sum_{m=1}^{\infty} k_s\, B_{ms}\, \sin\left(k_m x\right)\cos\left(k_s y\right)\exp\left(-\left({k_m}^2 + {k_s}^2\right)A_n(r)Dt\right) = -\left.\frac{\partial T(x,y,t)}{\partial y}\right|_{y}\end{aligned} \tag{72}$$

Therefore, the PD boundary conditions and initial condition are satisfied by the PD solution shown in Eq. (62).

5.2 Example 3: Solution for a Particular 2D Diffusion Problem with Dirichlet–Neumann Boundary Conditions

In this section, we consider a uniform initial condition $T(x, y, 0) = 100$ °C. The boundary conditions are shown in Eq. (57). Then,

$$B_{ms} = \frac{400}{LH}\int_0^L\int_0^H \sin\left(k_m x\right)\sin\left(k_s y\right)\mathrm{d}y\mathrm{d}x = \frac{800}{m(2s-1)\pi^2}\left(1-(-1)^m\right) \tag{73}$$

The PD solution is:

$$T_{\mathrm{pd}}(x,y,t) = \sum_{s=1,3,5\ldots}^{\infty}\sum_{m=1,3,5\ldots}^{\infty} \frac{1600}{ms\pi^2}\sin\left(k_m x\right)\sin\left(k_s y\right)\exp\left(-\left({k_m}^2 + {k_s}^2\right)A_n(r)Dt\right) \tag{74}$$

where $k_m = \frac{m\pi}{L}$, $k_s = \frac{s\pi}{2H}$, and $A_n(r)$ is given in Eq. (63). $r = \sqrt{\left(k_m\delta\right)^2 + \left(k_s\delta\right)^2}$. Note, k_s in Eq. (74) is different from the ones in other equations.

Let $L = H = 10$ cm, and $D = 1.14$ cm^2/s. The PD solutions at three different times ($t = 0.5$ s, $t = 4.0$ s, and $t = 8.0$ s) are calculated and presented in Fig. 10. We used the first 2500 terms in the PD series solution (m and $s = 1,2,\ldots,50$) for this example. In this figure, the classical solution and PD solutions with a relatively large horizon size $\delta = 0.4L$ are shown. Matching with the prediction from Fig. 8, the PD formulation corresponding to the kernel with $n = 0$, has a larger nonlocal effect compared with the other two cases; the one with $n = 2$ has the smallest nonlocal effect.

To further reveal the dependence of the nonlocal effect on the selection of the PD kernels, in Fig. 11, we calculate and show the temperature difference between the results from the PD solution with horizon size $\delta = 0.4L$ and the classical solution ($\delta = 0$). We notice that the initial heat flux singularities at the Dirichlet boundaries lead to relative large

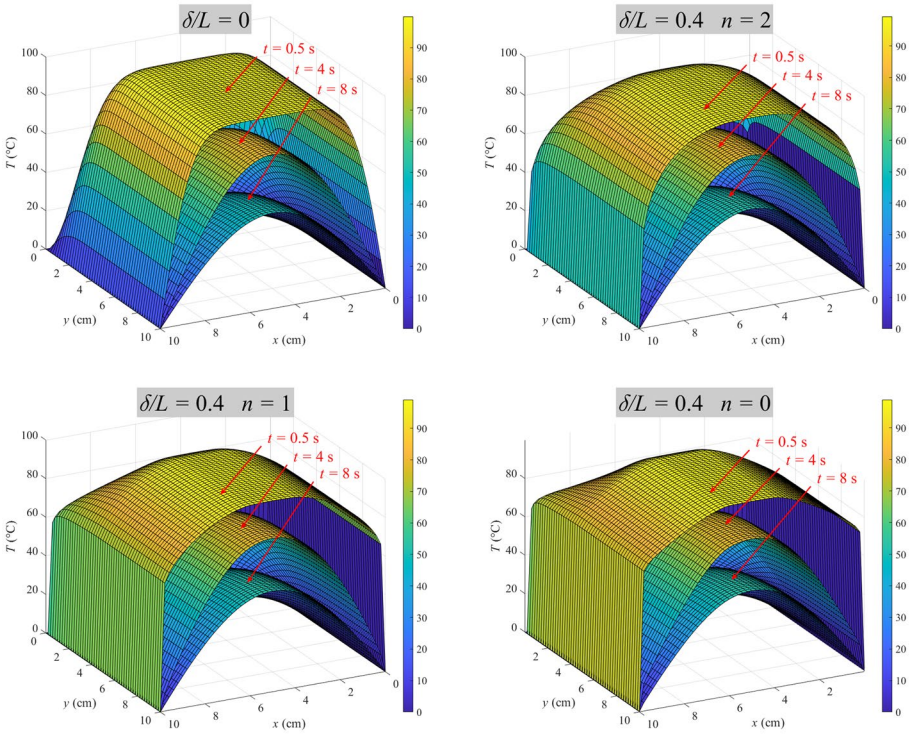

Fig. 10 Example 3: the snapshots of temperature profiles at times $t=0.5$ s, 4.0 s, and 8.0 s, from the classical solutions ($\delta/L = 0$) and PD solutions with horizon size $\delta = 0.4L$

difference at time $t=0.5$ s between the classical and the nonlocal models. The difference becomes smaller as time progresses.

In Fig. 12, we quantitatively show the effect of horizon size on the nonlocal effect. Only the PD formulation with $n=2$ is considered in this figure. Two horizon sizes, $0.1L$ and $0.01L$, are used. For these two horizon sizes, the shapes of the temperature difference profiles are almost the same, for each time snapshot. However, the temperature differences between the PD solutions corresponding to the $0.01L$ horizon size and the classical solution are about 100 times smaller than those corresponding to $0.1L$ horizon size.

6 Nonlocal Models Built Using Particular PD Nonlocal Factors

The PD analytical solutions obtained so far were based on a given kernel function. We have seen that those solutions can be built using corresponding solutions of the classical model by simply inserting a PD nonlocal factor ($A_n(r)$, where $r = k_m\delta$ for 1D, and $r = \sqrt{(k_m\delta)^2 + (k_s\delta)^2}$ for 2D) obtained based on the given kernel. A natural question is: given an arbitrary nonlocal factor (that converges to the classical solution when δ goes to zero), what is the corresponding kernel that is generated by it, and what are the properties of solutions obtained by using such a kernel?

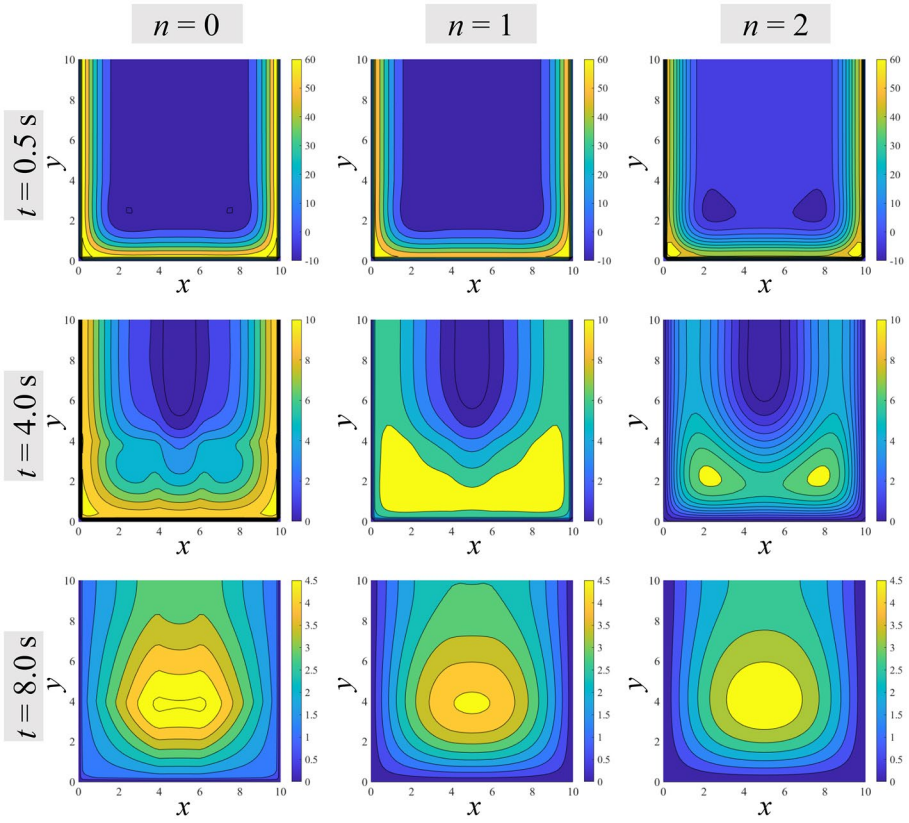

Fig. 11 Example 3: contours of the temperature difference between PD solutions with horizon size $\delta = 0.4L$ and the classical solutions, at times $t = 0.5$ s, 4.0 s, and 8.0 s

In this section, we answer these questions for a *particular* PD nonlocal factor in the 1D case: $A_p(r) = \frac{2(1-\cos r)}{r^2}$, $r = k_m\delta$. This particular nonlocal factor was selected to converge to the classical solution when δ goes to zero and be simple.

We employ this particular nonlocal factor into the 1D examples discussed in Sect. 3. Figures 13 and 14 show the temperature profiles at three different times, obtained with this particular nonlocal factor, for Examples 1 and 2 (Sects. 3.3 and 3.4), respectively. Four different horizon sizes are considered for the PD solutions. The classical solution is treated as a special case (horizon equal to zero) of the peridynamic solutions. Interestingly, the computed temperature profiles exhibit a step-wise behavior, in a double-level hierarchical structure. These solutions track closely the classical solution. When L/δ is an integer, e.g., $\frac{\delta}{L} = 0.05$ or 0.1 in Figs. 13 and 14, the widths of these steps match the corresponding horizon size. When L/δ is not an integer, e.g. $\frac{\delta}{L} = 0.03$ in Figs. 13 and 14, "sub-steps" appear within the main steps, and three-level hierarchical temperature profiles form. This type of dependencies on horizon size, domain geometry, and boundary conditions are also studied for elasticity problems in part II of this work [21], where an interesting behavior reminiscent of chaos in dynamical systems is noticed.

In spite of the step-wise behavior, the PD solutions obtained with this nonlocal factor do converge to the classical solution when the horizon size goes to zero, and the nonlocal effect

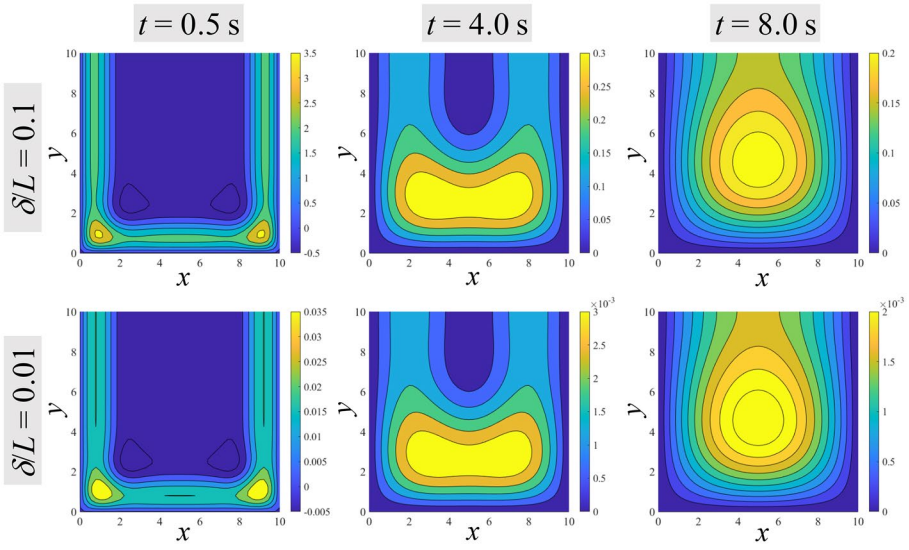

Fig. 12 Example 3: contours of the temperature difference between PD solutions with $n=2$ and the classical solutions, at times $t=0.5$ s, 4.0 s, and 8.0 s. Two horizon sizes are used: $0.1L$ and $0.01L$

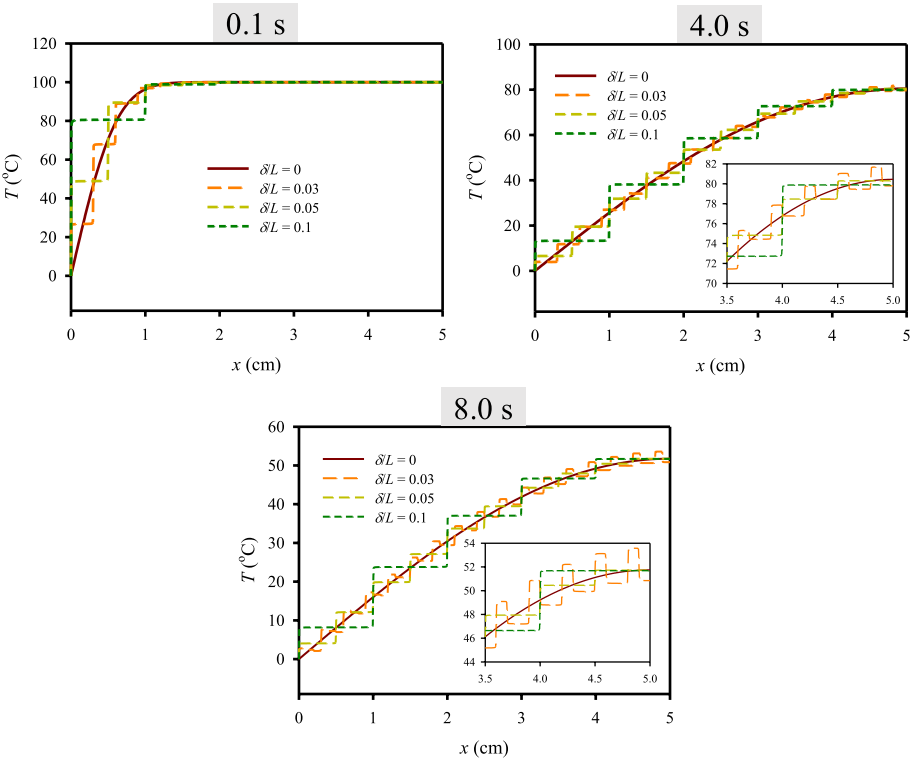

Fig. 13 Example 1: temperature profiles at times $t=0.1$ s, 4.0 s, and 8.0 s, from a PD model generated by the particular nonlocal factor $A_p(r)=\frac{2(1-\cos r)}{r^2}$. Only left half of the bar is shown

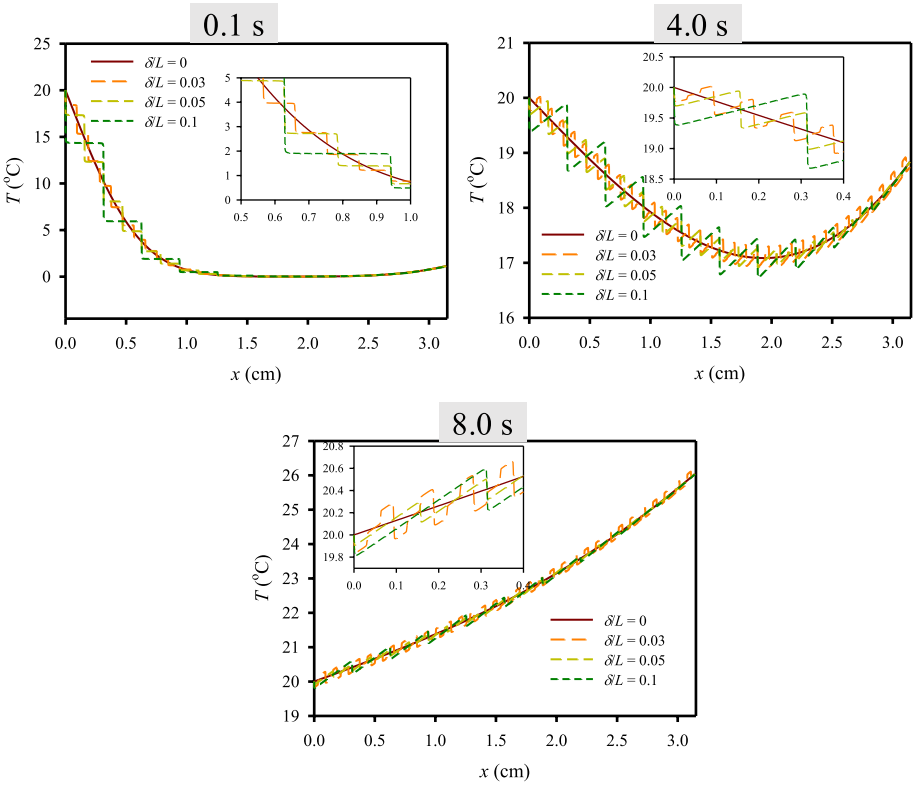

Fig. 14 Example 2: temperature profiles at times $t=0.1$ s, 4.0 s and 8.0 s, from a PD solution generated by the particular nonlocal factor $A_p(r) = \frac{2(1-\cos r)}{r^2}$

decays with time. Note that convergence of the infinite series solutions is slower with this nonlocal factor (which leads to step-wise temperature profiles): we used the first 4000 terms in the series to plot the results shown in Figs. 13 and 14. If a smaller number of terms are employed, one would notice wavy profiles (Gibbs-like behavior) around the "steps" in the temperature profile because of the stronger influence of the sine and cosine factors.

One can use Eq. (21) to now find the kernel function corresponding to the particular nonlocal factor. We show that the kernel corresponding to this particular nonlocal factor is:

$$\mu = \begin{cases} \frac{\mathcal{D}(\xi-\delta)+\mathcal{D}(\xi+\delta)}{\delta^2} & |\xi| \le \delta \\ 0 & |\xi| > \delta \end{cases} \tag{75}$$

where $\mathcal{D}$ denotes the *Dirac delta function*. Indeed, to verify this we use Eq. (21):

$$\begin{aligned} A(r) = \frac{\psi^\delta}{\psi^c} = \frac{\beta^\delta - \widehat{\mu}_k}{k_m^2} = \frac{-1}{k_m^2}\int_{-\delta}^{\delta} \frac{\mathcal{D}(\xi-\delta)+\mathcal{D}(\xi+\delta)}{\delta^2}[\cos(k_m\xi) - 1]\mathrm{d}\xi \\ = \frac{-1}{r^2}\int_{-\delta}^{\delta} [\mathcal{D}(\xi-\delta)+\mathcal{D}(\xi+\delta)][\cos(k_m\xi) - 1]\mathrm{d}\xi = \frac{2(1-\cos r)}{r^2} \end{aligned} \tag{76}$$

This kernel function has singularities at the horizon's edges and is zero elsewhere. The physical implication of this kernel is that each point is influenced only by points that are located exactly at the δ distance, and is not affected by other neighboring points located inside the horizon region. The unusual behavior observed in Figs. 13 and 14 is the result of this type of nonlocal interactions.

Remark: These observations lead to the possibility of generating specific kernels for specific PD models of material behavior. Indeed, one could find a PD nonlocal factor (therefore find a specific δ) by obtaining a best-fit of the analytical PD solution to a certain measured material response. This would then generate a corresponding kernel function, or constitutive relationship, that should be the best fit to that material behavior. This type of calibration method for PD models [43, 44] will be investigated in the future.

7 Concluding Remarks

It was generally assumed that finding exact solutions to the integro-differential equations generated by peridynamic (nonlocal) models would be, if not an impossible task, certainly a more complex proposition than finding solutions for corresponding classical partial-differential equations. Here, we dispelled this and showed that the separation of variable technique can be used for these nonlocal models in a very similar way to its use for finding exact solutions to PDE-based initial-boundary-value problems for transient diffusion.

We demonstrated how to directly obtain formal analytical solutions of peridynamic (PD) equations for transient diffusion problems (in 1D and 2D) based on existing series solutions of the corresponding classical (PDE-based) formulation by inserting a nonlocal factor, named here the "PD (nonlocal) factor," in the time-dependent part of the local series solution. The nonlocal factor depends on the horizon size and converges to one as the horizon size goes to zero, recovering the classical form of the solution for the corresponding PDE-based model.

We presented computing PD analytical solutions, for example, problems in 1D and 2D with Dirichlet and Neumann boundary conditions. We showed that, as time goes to infinity, the nonlocal solution converges, pointwise, to the classical one. In a particular case, we were able to show uniform convergence of the series solution using the Weierstrass test. We also showed that one can start with a particular peridynamic factor and discover new PD kernels with corresponding solutions that exhibit interesting horizon-scale structures.

The analytical peridynamic solutions derived here and their relations to the corresponding classical solutions are useful in selecting the horizon size in PD models as well as verifying computational methods for obtaining approximate PD solutions on simple domains.

Appendix 1. Separation of Variables for Classical Diffusion Initial and Boundary Value Problems

In this appendix, we briefly review the method of separation of variables for finding solutions to classical diffusion IBVPs, based on [22].

The 1D linear classical diffusion equation is:

$$\frac{\partial u(x,t)}{\partial t} = D\nabla^2 u(x,t) \tag{77}$$

We assume a solution in the form of the product $u(x,t) = \mathrm{X}(x)\mathrm{T}(t)$ and substitute in Eq. (77):

$$\mathrm{X}(x)\mathrm{T}'(t) = D\mathrm{T}(t)\mathrm{X}''(x) \tag{78}$$

where the single and double primes denote the first and the second order ordinary differentiation. Diving Eq. (78) by XT leads to:

$$\frac{1}{D}\frac{\mathrm{T}'(t)}{\mathrm{T}(t)} = \frac{\mathrm{X}''(x)}{\mathrm{X}(x)} \tag{79}$$

Since the left-hand side of Eq. (79) is a function of t only, and the right-hand side is a function of x only, we conclude that:

$$\frac{1}{D}\frac{\mathrm{T}'(t)}{\mathrm{T}(t)} = \frac{\mathrm{X}''(x)}{\mathrm{X}(x)} = \text{constant} = -k^2 \tag{80}$$

The minus sign in the constant comes from an educated guess, since a plus sign leads to an unreasonable form for the solution.

According to Eq. (80), a solution for the partial differential Eq. (77) must be a solution to the following pair of the ordinary differential equations (ODE):

$$\mathrm{T}'(t) + Dk^2\mathrm{T}(t) = 0 \tag{81}$$

$$\mathrm{X}''(x) + k^2\mathrm{X}(x) = 0 \tag{82}$$

The general solution for the ODEs is then:

$$\mathrm{T}(t) = \begin{cases} E & k = 0 \\ F\exp\left(-Dk^2t\right) & k \neq 0 \end{cases} \tag{83}$$

$$\mathrm{X}(x) = \begin{cases} Gx + H & k = 0 \\ I\sin kx + J\cos kx & k \neq 0 \end{cases} \tag{84}$$

where E, F, G, H, I, J, and k are constants to be determined. We then write the formal solution as the superposition of the cases where k is zero and nonzero:

$$u(x,t) = \mathrm{XT}|_{k=0} + \mathrm{XT}|_{k\neq 0} = C_1 + C_2x + \left(C_3\sin kx + C_4\cos kx\right)\exp\left(-Dk^2t\right) \tag{85}$$

where C_1, C_2, C_3, C_4, and k are all constants to be determined from initial and boundary conditions for a specific IBVP. Substituting BCs in Eq. (85) usually determines all possible k values and some of the other constants. Then, the solution is expressed as the superstition for all possible k's (usually includes a series if there are infinite number of k's). The initial conditions determine the remaining constants (see [22] for examples).

The 2D linear classical diffusion equation is:

$$\frac{\partial u(x,y,t)}{\partial t} = D\nabla^2 u(x,y,t) \tag{86}$$

We assume a solution in the form of the product $u(x,t) = \mathrm{X}(x)\mathrm{Y}(y)\mathrm{T}(t)$ and substitute in (86):

$$\mathrm{X}(x)\mathrm{T}'(t) = D\mathrm{T}(t)\left[\mathrm{X}''(x) + \mathrm{Y}''(y)\right] \tag{87}$$

Dividing by XYT leads to:

$$\frac{1}{D}\frac{\mathrm{T}'(t)}{\mathrm{T}(t)} = \frac{\mathrm{X}''(x)}{\mathrm{X}(x)} + \frac{\mathrm{Y}''(y)}{\mathrm{Y}(y)} = \text{constant} = \psi = -\left(k_1^2 + k_2^2\right) \tag{88}$$

And

$$\frac{\mathrm{X}''(x)}{\mathrm{X}(x)} = -\frac{\mathrm{Y}''(y)}{\mathrm{Y}(y)} - \left(k_1^2 + k_2^2\right) = \text{constant} = \varphi = -k_1^2 \tag{89}$$

Similar to the 1D case, only the negative signs for ψ and φ are used since the positive signs lead to unphysical solution forms.

Equations (88) and (89) give the three ODEs:

$$\mathrm{T}'(t) + D(k_1^2 + k_2^2)\mathrm{T}(t) = 0 \tag{90}$$

$$\mathrm{X}''(x) + k_1^2\mathrm{X}(x) = 0 \tag{91}$$

$$\mathrm{Y}''(y) + k_2^2\mathrm{Y}(y) = 0 \tag{92}$$

and the general solution for these ODEs are:

$$\mathrm{T}(t) = \begin{cases} E & \psi = 0 \\ F\exp(-D\psi t) & \psi \neq 0 \end{cases} \tag{93}$$

$$\mathrm{X}(x) = \begin{cases} Gx + H & k_1 = 0 \\ I\sin k_1 x + J\cos k_1 x & k_1 \neq 0 \end{cases} \tag{94}$$

$$\mathrm{Y}(y) = \begin{cases} My + N & k_2 = 0 \\ P\sin k_2 y + Q\cos k_2 y & k_2 \neq 0 \end{cases} \tag{95}$$

where E, F, G, H, I, J, and k are constants to be determined. We then write the formal solution as the superposition of all possibilities for zero and nonzero ψ:

$$\begin{aligned} u(x,y,t) &= \mathrm{XYT}|_{\psi=0} + \mathrm{XYT}|_{\psi\neq 0} \\ &= \mathrm{XYT}|_{k_1=0,k_2=0} + \mathrm{XYT}|_{k_1=0,k_2\neq 0} \\ &+ \mathrm{XYT}|_{k_1\neq 0,k_2=0} + \mathrm{XYT}|_{k_1\neq 0,k_2\neq 0} \end{aligned} \tag{96}$$

Similar to the 1D case, k_1, k_2, and other constants are determined from the initial and boundary conditions for a specific IBVP.

Appendix 2. Proof of Uniform Convergence for PD Solutions

In this appendix, we discuss uniform convergence of the formal PD solutions discussed in the paper. For the formal solutions shown in Eq. (27), we have:

$$\left|B_m \sin k_m x \exp\left(-DA_n\left(r_m\right){k_m}^2 t\right)\right| \leq C\exp\left(-DA_n\left(r_m\right){k_m}^2 t\right) \equiv N_m \tag{97}$$

Here, we used the fact that the sequence B_m is bounded from above by the integral of the absolute value of initial condition function g, which we assume is finite. C is a positive constant.

For $n=2$, we have,

$$A_2\left(r_m\right){k_m}^2 = \frac{2k_m}{\delta}\left[\mathrm{Si}\left(r_m\right) + \frac{\cos\left(r_m\right)-1}{r_m}\right] \tag{98}$$

When $m \to \infty$, we have $r_m \to \infty$, and,

$$\lim_{m\to\infty} \mathrm{Si}\left(r_m\right) = \mathrm{Si}(\infty), \text{a positive constant}$$

$$\lim_{m\to\infty} \frac{\cos\left(r_m\right)-1}{r_m} = 0 \tag{99}$$

Therefore, we can write:

$$\begin{aligned}
\lim_{m\to\infty}\frac{N_{m+1}}{N_m} &= \lim_{m\to\infty}\frac{C\exp\left(-DA_n\left(r_{m+1}\right){k_{m+1}}^2 t\right)}{C\exp\left(-DA_n\left(r_m\right){k_m}^2 t\right)} \\
&= \lim_{m\to\infty}\frac{\exp\left\{-Dt\frac{2k_{m+1}}{\delta}\left[\mathrm{Si}\left(r_{m+1}\right)+\frac{\cos\left(r_{m+1}\right)-1}{r_{m+1}}\right]\right\}}{\exp\left\{-Dt\frac{2k_m}{\delta}\left[\mathrm{Si}\left(r_m\right)+\frac{\cos\left(r_m\right)-1}{r_m}\right]\right\}} \\
&= \exp\left[-\frac{2Dt}{\delta}\mathrm{Si}(\infty)\left(k_{m+1}-k_m\right)\right] \\
&= \exp\left[-\frac{2Dt}{\delta}\mathrm{Si}(\infty)\frac{\pi}{L}\right] < 1
\end{aligned} \tag{100}$$

The ratio test shows that the series $\sum_{m=1}^{\infty} N_m$ is a convergent series of positive numbers. Now using Weierstrass M-test (see [22], page 875) in conjunction with the inequality (Eq. (97)) and the convergence of the series $\sum_{m=1}^{\infty} N_m$, we conclude that the series $\sum_{m=1}^{\infty} B_m \sin k_m x \exp\left(-DA_n\left(r_m\right){k_m}^2 t\right)$ converges uniformly.

Interestingly, following the same procedure as above, we get $\lim_{m\to\infty}\frac{N_{m+1}}{N_m} = 1$, for the PD solutions with $n=0$ or 1, so the ratio test for these cases is inconclusive, they may or may not converge uniformly.

An example of a case for which we do get convergence of the PD series solution is, for instance, when the initial condition function g is a constant, g_c. Indeed, if $g(x) = g_c$ we have:

$$B_m = 2\int_0^L g_c \sin k_m x\, dx = \frac{2g_c}{k_m}(1-\cos m\,\pi) \tag{101}$$

which leads to

$$B_{\mathrm{m}} = \begin{cases} \frac{4g_c}{k_m} m = 1,3,5\ldots \\ \\ 0 m = 1,3,5\ldots \end{cases} \tag{102}$$

and when $n=0$, we have

$$T_{\mathrm{pd}}(x,t)=\sum\nolimits_{m=1,3,5\ldots}\frac{4g_c}{k_m}\sin k_m x\exp\left(-DA_0\left(r_m\right)k_m^2 t\right) \tag{103}$$

where $\mathrm{A}_0\left(r_m\right)=\frac{6\left[1-\frac{\sin(r_m)}{r_m}\right]}{r_m^2}$. As $4g_c$ is a constant, we only need to consider the convergence of the series

$$S_{\mathrm{m}}=\frac{\sin k_m x}{k_m}\exp\left(-DA_0\left(r_m\right)k_m^2 t\right)=\frac{\sin k_m x}{k_m}E_m \tag{104}$$

Substituting the expression of $A_0\left(r_m\right)$, we get:

$$E_{\mathrm{m}}=\exp\left(-D\frac{6}{\delta^2}\left(1-\frac{\sin k_m x}{r_m}\right)t\right) \tag{105}$$

Since when $m\to\infty$, $E_m\to\exp\left(-\frac{6Dt}{\delta^2}\right)$ and $k_{\mathrm{m}}\to\infty$, we have

$$\lim_{m\to\infty}S_m=\lim_{m\to\infty}\frac{\sin k_m x}{k_m}E_m=0 \tag{106}$$

$$\lim_{m\to\infty}E_m=\exp\left(-\frac{6Dt}{\delta^2}\right) \tag{107}$$

We only need to prove that the series $\sum_{m=1,3,5\ldots}\frac{\sin k_m x}{k_m}$ converges. We apply Dirichlet's test to check the convergence of this series. Dirichlet's test states that if series $\left\{a_m\right\}$ and $\left\{b_m\right\}$ satisfy: (1)$a_m\geq a_{m+1}$; (2) $\lim_{m\to\infty}a_m=0$; (3)$\left|\sum_{m=1}^{\infty}b_m\right|\leq M$, where M is constant, then the series $\sum_{m=1}^{\infty}a_m b_m$ converges. Let us denote $a_m=\frac{1}{k_m}$ and $b_m=\sin k_m x$. Requirements (1) and (2) are easy to prove as follows:

$$\frac{1}{k_m}=\frac{L}{m\pi}>\frac{L}{(m+1)\pi}=\frac{1}{k_{m+1}} \tag{108}$$

$$\lim_{m\to\infty}\frac{L}{m\pi}=0 \tag{109}$$

For Requirement (3), we have:

$$\begin{aligned}\sum\nolimits_{m=1,3,5\ldots}^{N}\sin k_m x&=\sum\nolimits_{m=1,3,5\ldots}^{N}\sin\frac{m\pi x}{L}=\frac{\sin\frac{\pi x}{L}\sum_{m=1,3,5\ldots}^{N}\sin\frac{m\pi x}{L}}{\sin\frac{\pi x}{L}}\\&=\frac{\sum_{m=1,3,5\ldots}^{N}\left(\cos\frac{(m-1)\pi x}{L}-\cos\frac{(m+1)\pi x}{L}\right)}{2\sin\frac{\pi x}{L}}=\frac{1-\cos\frac{(N+1)\pi x}{L}}{2\sin\frac{\pi x}{L}}\\&\Rightarrow\left|\sum\nolimits_{m=1,3,5\ldots}^{N}\sin k_m x\right|\leq\frac{1+1}{2\sin\frac{\pi x}{L}}=\frac{1}{\sin\frac{\pi x}{L}}\end{aligned} \tag{110}$$

As shown above, the three requirements of Dirichlet's test for $\sum_{m=1,3,5\ldots}\frac{\sin k_m x}{k_m}$ are all satisfied for any x ($x\in(0,L)$). Therefore, the PD solutions in Eq. (103) converge.

The uniform convergence of PD solutions with $n=0$ or 1 remains to be further investigated in the future.

Appendix 3. Simplification of Ω^{δ} in 2D

To simplify ψ^{δ} in 2D (Eq. (54)), we will transform the double integral in the 2D nonlocal factor, $\psi^{\delta}(k_1,k_2)$, into a single integral, by noticing that $\psi^{\delta}(k_1,k_2)$ is a symmetric function of $r=r(k_1,k_2)=\sqrt{(k_1\delta)^2+(k_2\delta)^2}=\delta\sqrt{-\psi^c}$. Therefore, we can write $\psi^{\delta}(k_1,k_2)$ as $\psi^{\delta}(r)$.

Let $k_1\delta = r\cos\theta$, and $k_2\delta = r\sin\theta$, we have Eq. (54) as:

$$\psi^{\delta}=\int_0^{2\pi}\int_0^{\delta}\mu(R)\Big[\cos\Big(\frac{r}{\delta}\cos\theta\ R\cos\varphi\Big)\cos\Big(\frac{r}{\delta}\sin\theta\ R\sin\varphi\Big)-1\Big]R\mathrm{d}R\mathrm{d}\varphi \quad (111)$$

To prove that $\psi^{\delta}(k_1,k_2)$ is a symmetric function of $\sqrt{(k_1\delta)^2+(k_2\delta)^2}$, we only need to show that $\psi^{\delta}(r,\theta)$ is independent of θ. Let $\widehat{x}=R\cos\varphi$, and $\widehat{y}=R\sin\varphi$. We have:

$$\begin{aligned}\psi^{\delta}(r,\theta)&=\int_0^{2\pi}\int_0^{\delta}\mu(R)R\Big[\cos\Big(\frac{rR}{\delta}\cos\varphi\cos\theta\Big)\cos\Big(\frac{rR}{\delta}\sin\varphi\sin\theta\Big)-1\Big]\mathrm{d}R\mathrm{d}\varphi\\&=\int_0^{2\pi}\int_0^{r}\mu(R)R\Big[\Big(\cos\Big(\frac{rR}{\delta}\cos(\varphi+\theta)\Big)+\cos\Big(\frac{rR}{\delta}\cos(\varphi-\theta)\Big)\Big)/2-1\Big]\mathrm{d}R\mathrm{d}\varphi\end{aligned} \quad (112)$$

Since,

$$\begin{aligned}\int_0^{2\pi}\cos\Big(\frac{rR}{\delta}\cos(\varphi+\theta)\Big)\mathrm{d}\varphi&=\int_{\theta}^{\theta+2\pi}\cos\Big(\frac{rR}{\delta}\cos\varphi\Big)\mathrm{d}\varphi\\&=\int_{\theta}^{2\pi}\cos\Big(\frac{rR}{\delta}\cos\varphi\Big)\mathrm{d}\varphi+\int_{2\pi}^{\theta+2\pi}\cos\Big(\frac{rR}{\delta}\cos\varphi\Big)\mathrm{d}\varphi\\&=\int_{\theta}^{2\pi}\cos\Big(\frac{rR}{\delta}\cos\varphi\Big)\mathrm{d}\varphi+\int_{0}^{\theta}\cos\Big(\frac{rR}{\delta}\cos(\varphi+2\pi)\Big)\mathrm{d}\varphi\\&=\int_{\theta}^{2\pi}\cos\Big(\frac{rR}{\delta}\cos\varphi\Big)\mathrm{d}\varphi+\int_{0}^{\theta}\cos\Big(\frac{rR}{\delta}\cos\varphi\Big)\mathrm{d}\varphi\\&=\int_{0}^{2\pi}\cos\Big(\frac{rR}{\delta}\cos\varphi\Big)\mathrm{d}\varphi\end{aligned} \quad (113)$$

and, similarly,

$$\int_0^{2\pi}\cos\Big(\frac{rR}{\delta}\cos(\varphi-\theta)\Big)\mathrm{d}\varphi=\int_0^{2\pi}\cos\Big(\frac{rR}{\delta}\cos\varphi\Big)\mathrm{d}\varphi \quad (114)$$

we have,

$$\psi^{\delta}(r,\theta)=\psi^{\delta}(r)=\psi^{\delta}(r,0)=\int_0^{2\pi}\int_0^{\delta}\mu(R)R\Big[\cos\Big(\frac{rR}{\delta}\cos\varphi\Big)-1\Big]\mathrm{d}R\mathrm{d}\varphi \quad (115)$$

Therefore, $\psi^{\delta}(r,\theta)$ is independent of θ.

We further simplify $\psi^\delta(r)$:

$$\psi^\delta(r) = \frac{\delta^2}{r^2}\int_0^{2\pi}\int_0^r \mu\Big(\frac{\delta R}{r}\Big)R[\cos(R\cos\varphi)-1]\mathrm{d}R\mathrm{d}\varphi = 2\pi\frac{\delta^2}{r^2}\int_0^r \mu\Big(\frac{\delta R}{r}\Big)R\big[J_0(R)-1\big]\mathrm{d}R \tag{116}$$

where, J_0 is the zeroth-order Bessel function of the first kind. A change of variable $w = \frac{\delta R}{r}$ results in:

$$\psi^\delta(r) = 2\pi\int_0^\delta \mu(w)w\left[J_0\left(\sqrt{k_1^2+k_2^2}w\right)-1\right]\mathrm{d}w = 2\pi\widehat{\mu}_{\boldsymbol{k}} - \beta^\delta \tag{117}$$

where $\widehat{\mu}_{\boldsymbol{k}} = \int_0^\infty \mu(w)wJ_0\left(\sqrt{k_1^2+k_2^2}w\right)\mathrm{d}w$ is the Hankel transform of order zero for μ evaluated at $\sqrt{k_1^2+k_2^2} = \sqrt{-\psi^c}$, and $\beta^\delta = \int_0^{2\pi}\int_0^\delta \mu(w)w\,\mathrm{d}w\mathrm{d}\varphi$ is the integral of the kernel function.

Funding Z.C. and X.P. were supported by the Natural Science Foundation of China (No. 11802098). The work of S.J. and F.B was supported in part by the National Science Foundation under CMMI CDS&E award No. 1953346.

Declarations

Conflict of Interest The authors declare no competing interests.

References

1. Silling SA (2000) Reformulation of elasticity theory for discontinuities and long-range forces. J Mech Phys Solids 48:175–209
2. Silling SA, Epton M, Weckner O, Xu J, Askari E (2007) Peridynamic states and constitutive modeling. J Elasticity 88:151–184
3. Bobaru F, Zhang GF (2015) Why do cracks branch? A peridynamic investigation of dynamic brittle fracture. Int J Fracture 196:59–98
4. Ha Y, Bobaru F (2010) Studies of dynamic crack propagation and crack branching with peridynamics. Int J Fracture 162:229–244
5. Chen Z, Jafarzadeh S, Zhao J, Bobaru F (2021) A coupled mechano-chemical peridynamic model for pit-to-crack transition in stress-corrosion cracking. J Mech Phys Solids 146:104203
6. Chen ZG, Bobaru F (2015) Peridynamic modeling of pitting corrosion damage. J Mech Phys Solids 78:352–381
7. Jafarzadeh S, Chen ZG, Bobaru F (2018) Peridynamic modeling of repassivation in pitting corrosion of stainless steel. Corrosion-Us 74:393–414
8. Xu Z, Zhang G, Chen Z, Bobaru F (2018) Elastic vortices and thermally-driven cracks in brittle materials with peridynamics. Int J Fracture 209:203–222
9. Katiyar A, Agrawal S, Ouchi H, Seleson P, Foster JT, Sharma MM (2020) A general peridynamics model for multiphase transport of non-Newtonian compressible fluids in porous media. J Comput Phys 402
10. Seleson P (2014) Improved one-point quadrature algorithms for two-dimensional peridynamic models based on analytical calculations. Comput Method Appl M 282:184–217
11. Silling SA, Askari E (2005) A meshfree method based on the peridynamic model of solid mechanics. Comput Struct 83:1526–1535
12. Silling SA, Lehoucq RB (2008) Convergence of peridynamics to classical elasticity theory. J Elasticity 93:13–37
13. Lipton R (2014) Dynamic brittle fracture as a small horizon limit of peridynamics. J Elasticity 117:21–50

14. Bobaru F, Yang MJ, Alves LF, Silling SA, Askari E, Xu JF (2009) Convergence, adaptive refinement, and scaling in 1D peridynamics. Int J Numer Meth Eng 77:852–877
15. Mikata Y (2012) Analytical solutions of peristatic and peridynamic problems for a 1D infinite rod. Int J Solids Struct 49:2887–2897
16. Silling SA, Zimmermann M, Abeyaratne R (2003) Deformation of a peridynamic bar. J Elasticity 73:173–190
17. Wang LJ, Xu JF, Wang JX (2017) Static and Dynamic Green's Functions in Peridynamics. J Elasticity 126:95–127
18. Weckner O, Abeyaratne R (2005) The effect of long-range forces on the dynamics of a bar. J Mech Phys Solids 53:705–728
19. Silling SA (2016) Solitary waves in a peridynamic elastic solid. J Mech Phys Solids 96:121–132
20. Wang LJ, Abeyaratne R (2018) A one-dimensional peridynamic model of defect propagation and its relation to certain other continuum models. J Mech Phys Solids 116:334–349
21. Chen ZG, Peng XH, Jafarzadeh S, Bobaru F. Submitted. Analytical solutions of peridynamic equations. Part II: Elastic wave propagation
22. Greenberg MD (1998) Advanced engineering mathematics, Second Edition ed. Prentice Hall
23. Du Q, Gunzburger M, Lehoucq RB, Zhou K (2013) A nonlocal vector calculus, nonlocal volume-constrained problems, and nonlocal balance laws. Math Mod Meth Appl S 23:493–540
24. Aksoylu B, Gazonas GA (2020) On nonlocal problems with inhomogeneous local boundary conditions. J Peridyn Nonlocal Model 2:1–25
25. D'Elia M, Yu Y (2021) On the prescription of boundary conditions for nonlocal Poisson's and peridynamics models. arXiv preprint arXiv: 2107.04450
26. Foss M, Radu P, Yu Y (2021) Convergence analysis and numerical studies for linearly elastic peridynamics with dirichlet-type boundary conditions. arXiv preprint arXiv: 2106.13878
27. Zhao J, Jafarzadeh S, Chen Z, Bobaru F (2020) An algorithm for imposing local boundary conditions in peridynamic models on arbitrary domains. engrXiv: 7z8qr
28. Du Q, Gunzburger M, Lehoucq RB, Zhou K (2012) Analysis and approximation of nonlocal diffusion problems with volume constraints. Siam Rev 54:667–696
29. Chen ZG, Bobaru F (2015) Selecting the kernel in a peridynamic formulation: A study for transient heat diffusion. Comput Phys Commun 197:51–60
30. Chen Z, Bakenhus D, Bobaru F (2016) A constructive peridynamic kernel for elasticity. Comput Method Appl M 311:356–373
31. Gerstle W, Silling S, Read D, Tewary V, Lehoucq R (2008) Peridynamic simulation of electromigration. Comput Mater Continua 8:75–92
32. Oterkus S, Madenci E, Agwai A (2014) Peridynamic thermal diffusion. J Comput Phys 265:71–96
33. Silling SA, Bobaru F (2005) Peridynamic modeling of membranes and fibers. Int J Nonlin Mech 40:395–409
34. Kreyszig E (2017) Advanced engineering mathematics. John Wiley & Sons
35. Aksoylu B, Beyer HR, Celiker F (2017) Application and implementation of incorporating local boundary conditions into nonlocal problems. Numer Func Anal Opt 38:1077–1114
36. Aksoylu B, Beyer HR, Celiker F (2017) Theoretical foundations of incorporating local boundary conditions into nonlocal problems. Rep Math Phys 80:39–71
37. Aksoylu B, Celiker F (2017) Nonlocal problems with local Dirichlet and Neumann boundary conditions. J Mech Mater Struct 12:425–437
38. Aksoylu B, Gazonas GA (2020) On the choice of kernel function in nonlocal wave propagation. J Peridyn Nonlocal Model 2:379–400
39. Bobaru F, Duangpanya M (2010) The peridynamic formulation for transient heat conduction. Int J Heat Mass Tran 53:4047–4059
40. Piessens R (2000) The hankel transform. The transforms and applications handbook. CRC
41. Bobaru F, Duangpanya M (2012) A peridynamic formulation for transient heat conduction in bodies with evolving discontinuities. J Comput Phys 231:2764–2785
42. Olver FW, Lozier DW, Boisvert RF, Clark CW (2010) NIST handbook of mathematical functions. Cambridge University Press
43. Silling SA (2020) Propagation of a stress pulse in a heterogeneous elastic bar, Sandia Report. Sandia National Laboratories
44. Xu X, Foster JT (2020) Deriving Peridynamic Influence Functions for One-dimensional Elastic Materials with Periodic Microstructure. J Peridyn Nonlocal Model 2:337–351

Publisher's Note Springer Nature remains neutral with regard to jurisdictional claims in published maps and institutional affiliations.